2 mip

FINAL REPORT

"Experimental Investigation of the Critical Magnetic Fields of Transition Metal Superconductors"

1 June 1972 - 31 May 1973

Contract No. NAS 8 - 28900

Prepared by

Joseph P. McEvoy
Department of Physics
Clark University
Worcester, Massachusetts 01610

for

National Aeronautics and Space Administration
George C. Marshall Space Flight Center
Alabama 35812

Table of Contents

I. Introduction

The present research program had as its major goal the characterization of the critical fields of a type II superconductor. In particular, the research has been planned to clarify the determination (both experimentally and theoretically) of the maximum field at which the superconductive phase spontaneously nucleates in the bulk (H_{c2}) and on the surface (H_{c3}) of the metal.

Due to the great deal of theoretical interest in the temperature variation of H_{c2} and H_{c3}, the measurements reported here were originally designed to remove important discrepancies in the published literature of superconductivity. However, after a careful evaluation of previous experimental work of this nature, a new and important task was added. Simply stated, the problem was: "How does one reliably measure the surface nucleation field, H_{c3}?" In general, magnetic measurements of the bulk nucleation field, H_{c2}, had been determined and reported in the literature with reasonable consistency. Yet, the results for the surface nucleation field have been so inconsistent that it became necessary during this study to devote a significant portion of our effort to this question. The success we have had on this count constitutes one of the important breakthroughs of this research.

No theoretical work was completed (nor, indeed intended) during this study. However, the experiments reported here allow for the first time a definite choice between models.

II. Measurements and Materials

Most of the experimental techniques relating to this work have been developed in our laboratory during the NASA - sponsored research. Furthermore, none of this information has been presented in the quarterly reports. Thus, it is appropriate to describe in some details these experimental techniques in this section.

A.) DC Magnetization: Magnetization was directly measured by integrating the voltage produced by the changing applied field on an astatic coil pair. The pair consisted of two coils of carefully matched inductance, which were oriented to produce equal but opposite voltages in a changing field; the net

voltage is

$$V = \dot{\phi}_{net}/c \propto \dot{M} \qquad (1)$$

where $\dot{\phi}_{net}$ is the time derivative for the flux difference between the paired coils. This is proportional to M because flux changes due to the applied field alone produce cancelling voltages. The remaining voltage is due to the magnetization. This voltage was time integrated by the fluxmeter to produce an output proportional to the sample magnetization.

The integrator we used is an O. S. Walker Model MF - 2. An original prototype, this unit operates by use of a high grade operational amplifier with capacitive feedback. We have found experimentally that the integrator is capable of better than 2% accuracy over five-minute integration times.

The voltages integrated are quite small, requiring careful wiring and amplification. At typical sweep speeds (10 Gauss per second), the search coils we used produced an out-of-balance voltage of about .25 microvolts for a sample in the Neissner state. This voltage was dc and therefore indistinguishable from drift or a thermocouple voltage produced by a solder joint. The only way to prevent these spurious voltages from being integrated was to remove them at the source.

The integrator preamplifier must be carefully adjusted to zero output. Furthermore, thermocouple voltages were avoided by making the leads and coils from one continuous wire and letting the leads and the two solder joints at the integrator connector come to thermal equilibrium. This connector was left undisturbed for at least ten minutes before any data was taken. The leads to the coils were also allowed to reach thermal equilibrium.

The amplifier part of the integrator was a sophisticated chopper stabilized modulation demodulation circuit (modem). The input voltage was connected to a double-throw-double-pole chopper. One side of the chopper switched the signal from one side of a center-tapped Geoformer to the other. (A Geoformer is a very high inductance transformer designed to be used for the slowly varying voltages measured in geophysical applications.) The cycle of the input half of the chopper consisted of 40% in opposite polarities;in the time between these positions the contacts are shorted together to discharge the transformer. The other side of the chopper sampled this voltage for a short time compared to the cycle (10%) after the ringing transients have de-

cayed. The two sample voltages were mechanically rectified as illustrated in Figure 1. The circuit was similar to a box car integrator with a fixed gate.

The performance of the integrator is best described by its performance in a given situation and an explanation of the trade-offs. With the sensitivity set to 150 kilo-Maxwell turns full scale (This unit is easily converted to Gauss by dividing by the number of turns and multiplying by the area of the coil in square centimeters), the instrument had a sensitivity of 1 Gauss and was stable to within 1 Gauss over a three-minute integration time.

The probe and sample holder was of unique design, incorporating features to insure ease of sample placement, good thermal control, continuous and protected coils and leads, as well as ease of access.

The top assembly sealed the sample space of the cryostat and had feedthroughs for a tube to measure helium vapor pressure and for electronic connection. Attached to the top piece is an arm that extends down near the magnet to carry a third coil that picked off a radial component of the field to compensate for any difference between the two search coils in the cryostat. This feature allowed the coils to be balanced with the sample in the normal state without removing the probe from the cryostat. This arrangement differed from previous third coil compensators by being fixed to the probe rather than the magnet or cryostat, so it could be removed with the probe.

Two thin wall non-magnetic stainless steel tubes extend down from the top. The smaller tube (1/8th of an inch in diameter) carried the leads from the search coils. The other leads were braided together and were tied between the tubes with varnished silk thread. The larger tube (1/2 an inch in diameter) was used to measure the He vapor pressure.

The probe tip was designed to hold two sets of search coils and a carbon resistance thermometer. These were carried in a Stycast epoxy core that also had four Evenohm heaters embedded in it. Each hole for a coil was threaded at the bottom to take a brass plug that carried the sample. The samples were changed by simply unscrewing this plug. The four 60 ohm Evenohm wire heaters were bifilar wound, and placed between coil holes so the small magnetic moment of the wire would have equal, cancelling, effects on the search coils. (The heater wires are .001 inches in diameter.) The casting was poured in a cloth impregnated phenolic plastic cup. Except for a flange at the end to connect the tip to the rest of the probe, this plastic was machined away to leave as little around the epoxy (Stycast) as possible. A sleeve of styrofoam provided a small amount of insulation, enough to allow the heaters to warm the sample

above the transition temperature and not enough to take the smaple out of thermal contact with the bath. (It usually required about 10 joules of heat to heat the sample above T_c.) The probe tip is shown in Figure 2.

The care taken in this measurement was justified by the accuracy to which the magnetization defines the critical fields. The applied field was slowly varied (typically at 10 Gauss per second) and the sample was not disturbed in any other way. The voltage induced in the coils was proportional to the area into which flux penetrated. Variation of the field sweep rate has shown that the magnetization plots did not depend on the sweep rate for the values we used. Thus, these plots were of the bulk magnetization, precisely the kind of data for which H_c for type 1 material and H_{c1} and H_{c2} for type 2 material are defined. Later measurements of H_c, H_{c2} and H_{c1} using AC Susceptibility techniques were verified by their agreement with the magnetization data taken with the equipment described in this section.

B.) AC Susceptibility

At the outset of this research it was apparent that AC measurements of the magnetic susceptibility is the most promising technique for determining H_{c3}, the surface nucleation field. High sensitivity is available by null techniques with phase sensitive amplication and no leads need to be attached to the sample as in resistance measurements. In what follows, we outline the basic theory of the measurement.

B-1.) Theory of Susceptibility

It is helpful to consider the following: a long cylindrical sample is placed in AC field applied along the cylinder axis. The real part of the susceptibility is proportional to the "out of phase" voltage appearing in the secondary. Using Faraday's law

$$v'_{sec} = - N_{sec} \left(\frac{d\phi_{AC}}{dt} + \frac{d\phi_{DC}}{dt} \right) \qquad (2)$$

where N_{sec} is the number of turns of the secondary and ϕ_{ac} and ϕ_{dc} are the AC and DC components of the magnetic flux linking the secondary coil. Since only the AC component is detected by the bridge, then

$$\frac{d\phi_{AC}}{dt} = \frac{A dB_{AC}}{dt} = A \frac{dB_{AC}}{dH_{AC}} \frac{dH_{AC}}{dt} = A\left[1 + 4\pi \frac{dM_{AC}}{dH_{AC}}\right] \frac{dH_{AC}}{dt} \qquad (3)$$

where A is the cross-sectional area of the secondary coil. With $H_{ac} = h_o \exp(-i\omega t)$ we obtain from (2) and (3)

$$V'_{SEC} = i\omega NA\left[1 + 4\pi\chi'\right] H_{AC} \tag{4}$$

where $\chi' = \frac{dM_{AC}}{dH_{AC}}$

The frequency dependent magnetic susceptibility is defined as

$$\chi(\omega) = \chi'(\omega) + i\chi''(\omega) = \frac{\bar{M}}{H} \tag{5}$$

where M and H are complex. χ' gives a measurement of the differential susceptibility while χ'' is related to the energy dissipation in the sample. The imaginary argument "i" in equation 5 distinguishes the phase between the two components of the secondary voltage.

An "in phase" voltage v''_{sec} will occur in the secondary coil when power is dissipated in the sample. The time average rate of dissipation per unit volume is given by

$$Q = \left\langle -\bar{M}(\omega) \cdot \frac{d\bar{H}}{dt}(\omega) \right\rangle = \frac{1}{2} Im \left\langle \bar{M}(\omega) \cdot \bar{H}^*(\omega) \right\rangle \tag{6}$$

where $H(\omega) = h_o \exp(-i\omega t)$ is the exciting AC field. From $\chi(\omega) = \chi'(\omega) + i\chi''(\omega)$ we obtain

$$\bar{M}(\omega)\,\bar{H}^*(\omega) = \chi(\omega)\,\bar{H}(\omega)\,\bar{H}^*(\omega) = \chi(\omega)\left|H(\omega)\right|^2 \tag{7}$$

thus

$$Q = \frac{1}{2}\omega\left|H(\omega)\right|^2\chi''(\omega) \tag{8}$$

If v_n is the normal volume in the sample, then

$$Q\,V_n = \frac{1}{2} V_n\,\omega\,h_o^2\,\chi''(\omega) = I_p\,\Delta v_p \tag{9}$$

where I_p is the primary current and Δv_p is the change in the primary voltage coupled into the secondary, then

$$\Delta V''_{SEC} \propto \Delta V_p = \frac{1}{2}\,\frac{V_n\,\omega\,\chi''\,h_o^2}{I_p} \tag{10}$$

We can now understand the effect of the transition on the susceptibility signals. The "out of phase" voltage should increase as the flux starts to penetrate the sample and then level off as the normal state is reached. The "in phase" voltage $\Delta v''_s$ should increase as the flux penetrates and reaches a constant value in the normal state. Unually a peak is observed in χ'' as the sample goes from the completely diamagnetic to the completely normal state.

B-2.) Measurement System

A schematic diagram of the measurement system is shown in Figure 3. The sample was placed inside one of a pair of secondary coils wound astatically and coaxially with a primary coil. The primary provided the AC exciting field while the secondary was used as a sensor. Each secondary consisted of 664 turns of #40 wire and the primary of 1024 turns of #38 wire. The primary coils were about 30mm. long while the secondaries were about 5mm. long; thus the central part of the sample was probed and no end effects were introduced.

The primary coil was driven by a signal generated by an HR - 8 lock-in amplifier operating in its internal mode. When large amplitudes were desired, this signal was amplified with an EICO HF - 50 50 Watt wide band audio amplifier. Frequency variations from 46 to 2000 cycles and amplitudes from .25 to 3.5 Oe. were used for the driving AC field. The amplitude was monitored as the voltage drop across a 5Ω precision (1%) resistor connected in series with the primary circuit. This value was cross checked with a Hewlett Packard-456a Hall effect AC current probe. As the sample went through the transition, changes in the output voltage of the secondary were detected with a Complex Mutual Inductance Bridge balanced in the normal state. The values of the voltages in the secondary coil were measured with a PAR - 129 two phase lock-in amplifier, allowing one to monitor both the in-phase and quadrature voltages simultaneously. The DC field was generated with a 12 inch Spectromagnetic Industries Electromagnet (model 12-700) which could be rotated around the vertical axis. A Bell Model 610 Gaussmeter was used to measure the field and drive the x-axis of an 11" x 17" Moseley 7000AM x-y recorder. The Gaussmeter has a built-in calibration which was checked during each experimental run. Tracking error is estimated to be 1% of full scale reading.

The Mutual Inductance Bridge consists of two compensating networks used in balancing the secondary voltages in the normal state as shown in Figure 4. The "out of phase" or resistive component is balanced by a voltage across a 1 ohm resistor in series with a decade resistance divider. The "in phase" or inductive component is balanced by a voltage generated across a reference coil. The inductive voltage introduced into the detection circuit is proportional to the reading on the Gerstch Ratio Transformer Model R-7-61. On the other hand, the voltage in the resistive network is proportional to the dial setting on the resistance divider. The bridge provides for measurements with high sensitivity and precise phase resolution if care is taken to set the balance point.

Balance was accomplished in the following way. The field was increased until the metal was in the normal state. The bridge could then be balanced to zero for both components and any contributions due to the coils not being ideally astatic or flux linkage through the space between sample and coil were cancelled. Thus, changes in the susceptibility were measured with respect to the normal state.

For phase resolution, the phase angle between the "in and out of phase" components was adjusted with the PAR-129 to insure that the two components were orthogonal and therefore independent of each other. This was carried out by introducing an out of balance "in phase" voltage and tuning the phase angle of the lock-in for a minimum effect on the quadrature voltage. In general, no coupling between phases was detectable for instrument sensitivities necessary to accurately plot the superconductive transition. At low frequencies and amplitudes, the balancing procedure became tedious due to decreased signal to noise ratio.

The sample holder consisted of a cylindrical piece of phenolic in which the coil forms were inserted. The carbon resistor was attached to the outside of the cylinder. The primary and secondary leads were brought down through a stainless steel tube to shield them from stray inductances. The most important feature of the probe is a rod threaded into the phenolic that allows one to rotate the sample through the angle γ as shown in Figure 5. Since the electromagnet could be rotated through the angle θ, a very precise alignment of the field along the longitudinal axis of the sample could be achieved. To align the sample, the DC field was increased to a value corresponding to the middle of the superconducting-normal transition. The magnet was placed in a position close to the parallel configuration and the voltage v'_{sec} was monitored. As the magnet was rotated through the aligned position, the output voltage v'_{sec} went through a sharp minimum. A similar effect was observed if the sample was rotated with the rod through the angle γ. To understand why this minimum occurs it is important to recall that as the sample goes from the parallel to the perpendicular configuration, the value of the critical field H_{c3} shifts towards H_{c2}. In Figure 6 we present a plot of χ' in the vicinity of the transition for both the parallel ($\theta=\infty$) and perpendicular ($\theta=90^{o}$) configuration. If the angle θ is varied at constant applied field (for example the line AB in Figure 6), v'_{sec} will reach a minimum at B when the sample is perfectly aligned with the field. In Figure 7 the effect on v'_{sec} is shown as a function of the angle θ. The angular dependence is

quite sharp and from the figure it is observed that the sample could be aligned to within one-tenth of a degree.

C.) Cryogenics and Temperature Control.

A standard glass Dewar arrangement was used in the experiments reported here. An outer Dewar filled with liquid nitrogen reduced the heat entering the helium in the inside Dewar. A vacuum chamber separated the two jackets, which had to be evacuated down to 10^{-6} torr before each experimental run. The cryostat could be pressurized or evacuated to increase or decrease the helium vapor pressure and thus raise or lower the bath temperature. A temperature range from 1.2°K to 4.4°K was covered in this manner. During the course of the measurements reported here, some 49 separate transfers of liquid helium were necessary. At each transfer, approximately 2 liters was collected in the helium Dewar allowing a running time of approximately 6 hours.

The temperature was controlled with a manostat that operates on the principle of the Cartesian Diver. The manostat was opened first and the pressure reduced to the approximate value desired as measured by a manometer accurate to .5 torr. The manostat allowed for fine control in order to reach the desired value of the pressure. Usually the pressure varied in the first few minutes after adjustment, but after 5 minutes no measureable change in the pressure was observed. The manometer readings were calibrated with the 1958 He^4 Scale of Temperatures. In order to monitor variations in temperature near the sample, that might not be reflected in the manostat due to time lags, a carbon resistor was attached to the sample holder. Its resistance was measured with a Linear Research R-110 Picowatt AC Resistance bridge accurate to within .05%. This resistance was calibrated against the vapor pressure readings providing a crosscheck of the temperature. No significant changes in the resistor calibration was observed between runs. During each run the temperature was constantly monitored for significant changes in resistance or vapor pressure reading.

D.) Residual Resistivity Measurements.

A simple DC resistivity probe was constructed and is shown schematically in Figure 8. It consisted of an electrically insulated copper bed with a sensor for temperature determination. The sensor used was a Motorola HEP 36 transistor. It was forward biased with 100 microamps between the emitter and base. Since the voltage across the junction is linear in 1/T, we looked for a change in sensor voltage with no corresponding change in sample resistance

as the probe is lowered. When this condition was met, we were measuring the residual resistance of the sample. This resistance did not change until the temperature was low enough for the sample to become superconductive.

The resistivity was determined by the four terminal technique. The current was supplied by a Kiethley current source and the voltage was read with a Kiethley nanovoltmeter. The only complication in this measurement was a ground loop that gave anomalously high voltages. This problem was eliminated by using the nanvoltmeter in the battery mode.

The entire probe was designed to fit into an ordinary helium storage Dewar. Temperature was controlled by use of a heavy copper wire that dipped into the liquid helium. The length of the copper above the helium level determined an equilibrium temperature between the liquid helium and the heat leaked from the room temperature environment. The four leads were spot-welded to the sample and the sample was held in place with a rubber band.

E.) Sample Preparation.

For the measurements, we have chosen the alloy system tantalum-niobium as described in the original proposal. This system has normal state properties that enable us to cover the entire superconducting phase diagram without changing the lattice constant or the electron atom ratios of the material. It has the added advantage of forming a complete solid solution over the entire substitutional compositional range. The samples are mechanically stable under reasonably careful handling. Furthermore, the melting point of the samples exceeds 2000^{o}C so recrystallization at room temperature between measurements is unlikely. Tantalum is well known for its ability to resist oxidation and chemical attack, and does not absorb gases at room or low temperatures, so the surfaces will remain uncontaminated between experiments. These properties insure that the magnetic effects we see from different samples are entirely due to changes in the superconductivity as the field and the temperature are varied.

The desirable superconducting properties of the Ta-Nb system are its transition temperatures and its weak coupling behavior. The transition temperature of these alloys is about 4.5K, nearly the boiling point of helium at atmospheric pressure. It is thus possible to obtain reduced temperatures over most of the desired range by varying the He vapor pressure.

The intention of our sample preparation was to make the magnetization of the samples as reversible as possible without changing the surface properties of the material. Other workers have produced reversible magnetization data

by plating or oxidizing the surfaces. Yet, we have not done this because we wanted to study the surface sheath and compare its critical field with the bulk fields without intervening sample preparation.

The alloy samples were received spark machined to circular cross section. The magnetization showed that the samples were highly irreversible, trapping nearly all the flux that entered the samples when they were driven normal by the applied field. The surfaces were electro-polished in a solution of 9 parts reagent grade sulfuric acid to 1 part 48% hydrofluoric acid in a cell arrangement which is depicted in Figure 9. This treatment changed the nature of the irreversibility but did not eliminate it.

We next tried to reduce the irreversibility by cutting the ends to a conical shape. This was found to improve the reversibility of lead alloy samples by Gerard et.al.. Secula and Kernahan achieved an improvement in the reversibility of tantalum and niobium by cutting their samples to a prolate spherical shape. We chose the conical ends because they require minimal removal of metal. This was done with the Servo Met spark lathe at the U. S. Army Watertown Arsenal. The ends were chemical-polished in a solution of 3 parts nitric acid, 2 parts sulfuric acid and 2 parts of 48% hydrofluoric acid. This step further improved the magnetization but more preparation was clearly necessary.

The additional preparation was annealing. This is a difficult process for tantalum based alloys because of the combination of their high melting point and the tendency of hot tantalum to absorb residual gasses from the vacuum system. We used a vacuum of 4×10^{-7} Torr in a tube furnace at 1200°C for four hours. The annealed samples had a higher residual resistivity, indicating some gaseous impurities had been absorbed by the samples, but their reversibility improved enough that the remnant magnetization of the samples was unmeasurably small at 4.2K.

III. Experimental Results

In this section of the report is presented the major experimental data bearing on the original purpose of the investigation, the temperature variation of the critical fields of type II superconductors. As outlined in our original proposal, careful tests of theoretical predictions of the temperature dependence of the critical fields require precise and unambiguous experimental determinations. Such tests were the major goal of the present study. It soon became apparent that it was necessary to review in a fundamental way

the various criteria which had been used by previous investigators to determine the critical fields, particularly at bulk and surface nucleation. This forms a significant portion of the experimental results.

A.) Criteria for Determination of Critical Fields

1) DC Magnetization.

As described above under "Measurements and Materials", DC magnetization techniques produce a low-level DC voltage proportional to the bulk diamagnetism of the sample. There are several disadvantages of this technique although the information obtained is, for the most part, unambiguous. The major problem, integrator drift, leads to large errors at the nucleation fields since the superconductivity is vanishing at these points. Furthermore, DC methods are inherently less sensitive than AC due to the present availability of AC instrumentation employing signal-averaging schemes. Another disadvantage of DC susceptibility relative to its AC counter-part is the lack of phase information which is extremely important in detecting the superconducting normal transition at the surface nucleation field, H_{c3}. One final positive word regarding DC susceptibility: there is no doubt about what one is observing. In measuring large samples, the temperature variation of the bulk nucleation field $H_{c2}(t)$ can be determined unambiguously. These results can be used to check AC data which are subject to some interpretation, as shown in what is to follow.

2) AC Susceptibility

The general features of the susceptibility curves are quite reproducible and easily described. Typical χ' and χ'' curves are presented in Figure 10, for small frequency and amplitude of the applied AC field. The χ' curve which measures the differential susceptibility, is seen to go through a sharp decrease as the applied DC field is lowered from the normal state. A minimum constant value is reached at low fields (Meissner State). The χ'' curve, which measures the energy dissipation in the sample, is seen to rise sharply above the normal state as H is lowered and drops to a value below the normal state at low DC fields. These data points were reproducible and reversible when taken under static conditions, i.e. at constant applied field. On the other hand, if the field was swept a large hysterisis was introduced, as shown in Figure 11. We should note that for large values of h_o (4.0 gauss) and (1000 Hz.), the hysterisis is greatly reduced. At present there is no clear understanding of this effect.

As the magnitude of the exciting field h_o and frequency were changed, both χ' and χ'' were affected as shown in Figures 12-14. At low values of h_o the peaks in χ'' were very sharp and occured close to H_{c3}. As h_o was increased, the peaks broadened and shifted towards H_{c2}. The same broadening is observed in the χ' curves. As the frequency was increased, the position of H_p (the peak field in χ'') approached H_{c3} as shown in Figure 14. The relative values of the peak heights and the change in χ' were strongly dependent on the frequency.

It is interesting at this point to compare the χ' curve to what would be expected from DC magnetization data. In Figure 15 a plot of the DC magnetization and susceptibility is presented for the Ta-Nb 4% alloy. Here the values of χ' are obtained by graphically differentiating the magnetization curve. It is seen that the values differ widely from those observed experimentally from AC susceptibility. This difference is due to the fact that DC magnetization measures average bulk properties of the sample. The AC measurements only probe the surface region due to the screening currents in the sheath that shield the bulk. This has caused much confusion in the published literature on AC susceptibility of superconductors.

A number of experiments have been performed to determine the critical fields of superconductors using AC susceptibility techniques. However, the criteria used to determine the critical fields from the data varied widely from experiment to experiment, and no attempt has been made to clarify the situation. This is demonstrated in Table I where a review of the various criteria used by different researchers is presented. In what follows, we present suggestions for universal criteria and justify these choices with systematic experimental data.

Recall in Figure 7, the plot of χ' versus the angle between the applied field and the sample axis. From this figure we could pick various points from both the perpendicular and parallel field configurations to indicate the transition point H_{c2}. At $\theta = 0$ (parallel case), the transition is rather broad and no clear identifying point can be chosen. However, at $\theta = 90$ (perpendicular case), no sheath is present and the transition for χ' is much sharper. Though some rounding is present as the sample goes into the Meissner state, the sudden drop in χ' indicates a very basic change in the bulk properties. We found no change in the value of H_{c2} as determined by this criteria if the AC field amplitude or the frequency are varied. The validity of this criterion is further confirmed by the susceptibility curves obtained at high values of

the exciting AC field h_o as shown in Figure 16. The large AC field is able to penetrate the bulk through the screening currents and produces changes in both χ' and χ'' curves at H_{c2}. If the value of H_{c2} is taken to be the point at which the breaks occur in χ' and χ'', very good agreement is found (1%) with the value obtained from the low AC field criteria. This leads us to conclude that the true measurement of the bulk critical field is obtained by measuring χ' in the perpendicular configuration at low AC amplitudes and taking H_{c2} as the field at which χ' decreases sharply.

For determining H_{c3}, the situation is more complicated. Since 1963, when St. James and de Gennes first predicted the existence of the surface sheath, experimentalists have used different features in various physical measurements as the true H_{c3}. The most obvious choice of H_{c3} from AC susceptibility data is to take the field at which χ' or χ'' first departs from the normal state value. When this criterion is applied, the value of H_{c3} from χ' (at constant h_o and ω) is lower than that from χ'' by as much as 5%. Since the detection of the losses in the sheath is expected to be more sensitive than the slope of the magnetization, the value obtained from the χ'' curve should be a more accurate value. This has been generally accepted in the recent literature. However, we have found the value obtained by this criterion to be strongly frequency dependent at low reduced temperatures.

In 1971 Hopkins suggested as a criterion the point at which the extrapolation of the normal state value and the linear part of the peak in χ'' intersect. This criterion could be easily applied to our low h_o data, but became less accurate for high h_o. However this criterion also yields a strongly frequency dependent H_{c3}. The dependence observed is similar to that obtained by Hopkins for pure Niobium. H_{c3} varied linearly with frequency up to a certain value at which H_{c3} seemed to level off and remain constant, as shown in Figure 17.

In 1966 Doidge[27] suggested that since the peak shifts to H_{c3} as h_o is decreased, then if the peak value H_p in χ'' is plotted as a function of h_o, an accurate value of H_{c3} might be obtained. When H_p^2 is plotted versus h_o for low h_o, fairly straight lines are obtained. If they are extrapolated to $h_o = 0$, a frequency and amplitude independent value of H_{c3} is obtained. We have obtained $H_{c3} = 926 \pm 15$ gauss at 3.4 K from the data shown in Figure 18. This value is within experimental error and this criterion seems to be the most effective in the determination of H_{c3}.

This completes the discussion of the criteria used in determining the

critical fields of these superconducting alloys. In the next section we present the actual measurements of the temperature variation of the bulk and surface nucleation fields, as determined from the criteria described above.

B.) Measurements of Bulk Nucleation Field, H_{c2}.

In the previous section, we have described how the AC susceptibility measurement is utitized to measure the bulk nucleation field, H_{c2}. Since the AC data was in extremely good agreement with the DC magnetization, we present here the values of $H_{c2}(T)$ taken from χ' at an angle of 90° (see Figure 7). In Figure 19, a plot of $H_{c2}(T)$ versus T is presented for a tantalum ± 4% niobium alloy. These data were obtained from AC susceptibility as described in section III-A. From the value of the slope, $dH_{c2}/dT|_{T_c}$, we can obtain a value for the Fermi velocity from the modified Gor'kov expression:

$$\langle v_F^2 \rangle = \frac{24\pi^2 k_B^2 T_c^2 \eta}{7\zeta(3) e\hbar \left| \partial H_{c2}/\partial t \right|_{t=1}} \qquad (11)$$

It is gratifying to know that the value of v_F obtained from this equation (i.e. completely determined by the superconductivity of the metal), is within 10% of the average v_F computed from band structure calculations of Matthies and co-workers. This constitutes the completion of an important goal of the research, as outlined in the original proposal. We evaluate $dH_{c2}/dT|_{T_c}$ = 545 gauss/degree from this curve, in good agreement with the values obtained on this sample by DC magnetization. However, the values are in wide disagreements with those of Kubota et al in a similar alloy, although a discrepancy in concentration may account for the difference. Careful chemical analysis of the composition of our sample will be carried out upon completion of these studies.

C.) Measurements of the Surface Nucleation Field - $H_{c3}(T)$.

As we have discussed in section III, there are various criteria which could be employed to determine the value of H_{c3} at a given temperature. Our unique method, which makes use of the amplitude dependence of the peak field in χ'', appears to be the most reliable. This fact constitutes an important new result from this work. In addition to determining H_{c3} by this method however, we have also used the more conventional other two criteria in order to make a reasonable comparison. In Figure 18 the H_{c3} versus T data is plotted for the three criteria we have discussed in section III. At high temperatures (i.e. close to T_c) the three criteria do not differ, but at low temperatures

large changes occur and three different lines can be drawn through the data points.

If we define the critical temperature from the extrapolation to H = 0 of the H_{c3} and H_{c2} data, no unique temperature is defined, in agreement with previous experiments. The lower value of T_c obtained from the H_{c3} extrapolation implies a difference in critical temperature between the surface sheath and the bulk. This effect could be due to a higher κ value on the surface of the sample.

We have compared our experimental results with the Sarma[12] theory with no quantitative agreement, as shown in Figure 20. The experimental results fall below both the p = 0 and p = 1 curves. It should be pointed out that disagreement with the theory occurs for all three criteria used over the whole temperature range covered in these experiments.

The experimental data presented in Figure 19 allows us to form the ratio H_{c3}/H_{c2} and determine the temperature dependence of this important quantity. This is an important goal of the present work as outlined in the original proposal.

The ratio H_{c3}/H_{c2} was found to vary widely over the temperature range studied for all three criteria outlined above, as shown in Figure 21. Data is presented for all three criteria; the points corresponding to the H_p^2 versus h_o criterion were obtained from the straight line drawn through the experimental data points. It is not possible to draw definite conclusions from the data available until the range up to $4.47^{\circ}K$ can be studied and the H_p^2 versus h_o criteria is applied to the whole temperature range. We have found that qualitatively the shape of the curves follows the general shape of the theoretical predictions of Indovina et al. It can be seen that all three curves seem to be leveling off as the temperature is reduced. The Indovina theory predicts that as $t = T/T_c$ goes to zero, H_{c3}/H_{c2} should approach 1.695. The first two criteria will not agree with this prediction while the third one seems to be approaching this value.

It should be pointed out, that we do not expect one theory to exclude the other one. It is possible that near T_c the boundary effects will be of more importance than scattering at the surface. At low temperatures, scattering effects might play an important role, in which case the two limits might fit each theory separately while in the intermediate ranges a combination of the two might prove to be necessary. From the qualitative agreement of the data, it is possible to say at this point that a clearer picture of the tem-

perature dependence of $C(t) = H_{c3}/H_{c2}$ from the theoretical point of view is now available.

In the process of performing these experiments (alignment, etc.), we have also recorded the angular dependence of H_{c3}. It is appropriate to discuss those measurements at this point. We have measured the angular dependence of H_{c3} from $\theta = 0^{\circ}$ to $\theta = 90^{\circ}$ as shown in Figure 22. These results can be immediately compared to theory, as St. James has solved the Ginzburg-Landau equations for the sheath nucleation as the angle θ between the applied field and the sample is varied from the parallel to the perpendicular field configuration. The differential equation obtained when this problem is considered can not be solved, but an approximation is possible for small angles. The result obtained is

$$\frac{dH_{c3}(\theta)}{d\theta} = -1.4\ H_{c3} \qquad (12)$$

The theoretical initial slope of $dH_{c3}(\theta)/d(\theta)$ should extrapolate to $\theta = 22^{\circ}$ according to theory. Our initial slope extrapolates to $\theta = 20^{\circ}$, which is very good agreement if the approximate nature of the solution is taken into account. Since the criteria at low temperature was not definite, this experiment was carried out at $4.2^{\circ}K$ where H_{c3} was well defined.

D.) Field Dependent Susceptibility

In this section we report on experiments which were not originally proposed. However, the measurements were performed as part of the present investigation and are so fundamental to the main conclusions that they are included in the report.

Before the experimental data is presented however, it is necessary to review briefly the theoretical understanding of the problem. At present there is no detailed microscopic theory that describes the response of a superconductor to an applied AC field between H_{c2} and H_{c3}. Recently, Callarotti et al have proposed a phenomenological theory that considers the response of a cylindrical sample in this region. They consider the classical electromagnetic response of an inner normal core of conductivity, σ_n, covered by a layer of thickness and effective consuctivity, σ_s. They further assume that the sheath effective conductivity depends quadratically on x, where $x = (H_{c3} - H)/(H_{c3} - H_{c2})$, and inversely proportional to the amplitude of the applied AC field, h_o. Callarotti et al use the field dependent sheath thickness

given by Fink and Kessinger. The basic derivations of the theory are presented in the papers of Callorotti, while comparison of experimental results with the model will be presented in this section. For convenience in comparing the experimental results to the model, we will refer to the real and imaginary parts of the magnetic permeability in M.K.S. units, μ' and μ''. The susceptibility and permeability are related by the following

$$\chi' = \mu' - 1 \tag{13}$$

and

$$\chi'' = \mu'' \tag{14}$$

The model predicts that the real and imaginary compononets of the permeability are given by

$$\mu' = \frac{\mu'_N}{1 + 2y\mu''_N + y^2\left[\mu'^2_N + \mu''^2_N\right]} \tag{15}$$

and

$$\mu'' = \frac{\mu''_N + y\left[\mu'^2_N + \mu''^2_N\right]}{1 + 2y\mu''_N + y^2\left[\mu'^2_N + \mu''^2_N\right]} \tag{16}$$

where μ'_N and μ''_N are the normal state permeabilities and y is given by

$$y = \frac{1}{2}\frac{D_o}{a}\frac{D(x)}{D_o}\left[x^2\right]\left[ka\right]^2\delta\frac{1}{h_o} \tag{17}$$

where

$D(x)$ = Thickness of the sheath

$D_o(x) = D(x)\big|_{x=o}$

$$x^2 = \{H_{c3} - H\}/\{H_{c3} - H_{c2}\} \tag{18}$$

a is the radius of the sample

$$k = \sqrt{\mu_o \omega \sigma_N} \tag{19}$$

and δ is a frequency independent constant. We can see in (14) that μ'' will have a maximum at $y = y_p$, where y_p is given by

$$y_p = \frac{\mu'_N - \mu''_N}{\mu'^2_N + \mu''^2_N} \tag{20}$$

and the value of the permeability at the peak will be given by

$$\mu''(y_p) = \mu''_{MAX} = \frac{1}{2}\,\frac{\mu'^2_N + \mu''^2_N}{\mu'_N} \tag{21}$$

and therefore μ''_{max} (value of χ'' at the peak) should be independent of h_o and the DC field, and depend only on the normal core properties (ω, a, σ_N). Furthermore, since at fixed frequencies μ'_N is constant, the change in μ' at constant frequency should be the same for all h_o. In Table II a comparison of this prediction is presented. Since $\mu' \propto v'_{sec}/h_o$ and $\mu'' \propto v''_{sec}/h_o$, the values are obtained by dividing the peak and $\Delta v'_{N-S}$ voltages by the applied AC field. We have found agreement with this prediction to within 3.5%.

If we now consider (17) at the peak and at constant ka (constant frequency), then

$$y_p = \frac{1}{2}\,\frac{D_o}{a}\,\frac{D(x)}{D_o}\,x_p^2\,[ka]^2\,\frac{\delta}{h_o} \tag{22}$$

and close to H_{c3} ($x \simeq 0$) then $D(x) \simeq D_o$, and from this we can see that only x_p and h_o will change, and we can write

$$x_p^2 = \text{constant}\ h_o \tag{23}$$

We have plotted this prediction in Figure 23. Note that since $x_p^2 = \{H_{c3} - H\}^2/\{H_{c3} - H_{c2}\}^2$, the denominator is a constant and we can rewrite (23) as

$$H_p^2 = \text{constant}'\ h_o + H_{c3} \tag{24}$$

which is equivalent to the criterion used in the determination of H_{c3} described in the previous section. <u>This supports the validity of that procedure, and constitutes an important result of this work</u>.

According to the theory, if experimental results for μ' and μ'' are plotted against the variable y, then at constant frequency, all curves at different h_o should coalesce into a common curve given by equations (13) and (14). In Figures 24-27, experimental results are presented comparing μ' and μ'' to the theoretical prediction. It is important to note that in the generation of these curves, the experimental value of the residual conductivity is used. We have used the value obtained by Weber accurate to only 10%. The theoretical curves depend strongly on this value near H_{c3}.

We now wish to compare the experimental results with the theoretical mod-

el just outlined. We first note that the agreement is similar for all values of ka (frequency) studied which ranged from .26 to 1.21. Near H_{c3} the agreement seems to be good; as y increases the agreement remains good up to y = 1.2 where wide disagreement is observed. Callarotti et al observed somewhat better agreement in Niobium samples near H_{c3} with discrepancies observed starting at a value of y = 4. This disagreement near H_{c2} is probably due to changes in the bulk properties as the mixed state is approached.

The small discrepancies observed are not due to experimental errors in these measurements, but they are perhaps due to one of several sources. First, as mentioned previously, the value of the normal conductivity has a strong effect on the theoretical curves. Thus, a more accurate measurement of this value should be made. Secondly, the assumed effective conductivity form for the sheath might be different for our sample, the model having been developed for Niobium. A third source of difficulty could be the field dependence of the sheath thickness. We have used the dependence predicted by Fink and Kissinger from solutions to the Ginzburg-Landau equations using $\partial\psi/\partial x = 0$ as the boundary condition. Experimental evidence leads us to conclude that a less restrictive boundary condition is more appropriate. A change in this boundary condition should have an effect on the thickness of the sheath predicted by theory.

IV. Conclusions and Further Experiments.

The isothermal magnetic transitions of a type II superconductor ($\kappa = 1.0$) have been studied by AC susceptibility techniques as a function of the amplitude h_o and frequency of the exciting field. The field variation of the complex susceptibility $\chi(\omega) = \chi'(\omega) + \chi''(\omega)$ is used to determine the critical fields. We have observed that the ratio H_{c3}/H_{c2} is depressed below the St. James DeGennes value for temperatures near T_c, in qualitative agreement with the recent prediction of Indovina et al. H_{c2} is taken as the field which restores the normal state value of χ' in a perpendicular field. H_{c3} on the other hand, is more difficult to select since the criteria used by previous workers yields frequency dependent values. We have shown that $H_{c3}(T)$ determined from the peak in χ'' for vanishing small values of h_o yields a frequency independent value. The functional relationship obtained from $\chi''_p(h_o)$ is found to be precisely that contained in the recent phenomenological model proposed by Callarotti et al. Experimental curves of χ' and χ'' are compared to those predicted by the

Callarotti et al model. The agreement is good except near H_{c2} where some important corrections are to be expected.

It is clear that some experiments are needed before certain conclusions can be drawn, but at this point, we can make definite statements about our investigations.

The criteria to measure the bulk critical field H_{c2} from the χ' curve in the perpendicular field configuration has proven to be accurate and no change was observed when the frequency and amplitude were varied. Both experimental and theoretical evidence seem to give weight to the H_p^2 versus h_o criterion for determining H_{c3}. However, further experiments on the frequency and amplitude effect on H_{c3} as determined from other criteria should be performed. We suggest that these tests be carried not only in the Ta-4% Nb sample, but for other alloys with different κ values and the pure metals Tantalum and Lead. Surface condition should also be changed in studying the frequency dependence of H_{c3}.

The H_{c3}/H_{c2} values should be extended for lower and higher temperatures in Ta-Nb 4%. This would enable us to compare the results near T_c to the Indovina et al results and establish the validity of the Hu and Koreman theory by measuring the value of the ratio as $T \to 0$.

Once a definite criteria is established for the measurment of H_{c3}, and an accurate value of the conductivity is obtained, a better comparison to the Callarotti model will be possible. Furthermore, if both χ' and χ'' are measured at a temperature at which the ratio $H_{c3}/H_{c2} = 1.695$, the uncertainties on the values of the sheath thickness would be eliminated. Modifications of the sheath conductivity near H_{c2} might combine with the available model to produce a complete explanation of the observed susceptibility curves. This would lead to a better microscopic understanding of the effects that produce this effective conductivity on the sheath.

The only discussion in the literature as to the choice of criteria is F. de la Cruz, M.D. Maloney and M. Cardona, Phys. Rev. 187, 766 (1969).

D. Saint James, Physics Letters 16, 218 (1965).

H. J. Fink and R. D. Kessinger, Phys. Rev. 140, A1937 (1965).

Statistical Physics, L. D. Landau and E. M. Lifshitz, Pergamon Press, London (1966).

L. P. Gorkov, JETP (USSR) 34 735 (1958), translation, Jetp, 7, 505 (1958).

Methods of Mathematical Physics, P. M. Morse and H. Fesbach, McGraw-Hill, New York, 1953.

Handbook of Mathematical Functions, Edited by M. Abramovitz and I. Segun, Dover Publ. Inc., New York (1970), p. 379 and 430.

LIST OF TABLES

TABLE I

Review of the criteria used in determining critical fields

AUTHOR		H_{c3}	H_{c2}
Bertman and Strogin	16	Peak in χ''	No mention
Rollins and Silcox	17	Critical currents-vs-Field	χ' at low h_o and H_o
Hopkins	18	breaks in χ'', χ'	χ'' peaks
Maloney et al	19	χ' at three different points	χ' at 90
Ostenson and Finnemore	20	Sharp break in χ''	χ' peaks
Rollins and Cappaletti	21	χ' and χ'' as both go to normal state	χ'' peak at large H_o
Akmedov	22	No mention	No mention
Callarotti	23	break	χ' at 90
Strongin and Paskin	24	No mention	No mention
Van Engelen	25	No mention	No mention
Karasik	26		
Doidge	27	H_p^2 vs. H_o	

TABLE II

Frequency (Hz.)	h_o (gauss)	$\chi' \propto \frac{\Delta V'_{sec}}{h_o}$	$\chi''_p \propto \frac{V''_{secp}}{h_o}$
46	1.33	4.73	2.12
"	.663	4.80	2.06
"	.348	4.69	1.90
"	.174	4.76	1.98
100	.348	9.48	3.72
"	.174	9.48	3.88
"	.0830	9.57	4.00
1200	3.15	28.3	12.4
"	2.24	28.4	12.5
"	1.33	27.9	12.3
"	.663	27.5	12.5
"	.348	28.2	12.4
"	.174	27.6	12.3
"	.0829	27.7	12.5
500	.0829	45.8	20.6
"	.348	46.8	20.1
"	.663	47.0	20.4
"	1.33	46.6	20.3
"	2.24	45.6	19.7
"	3.15	46.6	20.1
1000	3.06	75.8	31.6
"	2.23	77.0	31.5
"	1.32	76.1	32.0
"	.663	77.1	31.7
"	1.30	75.0	32.0
"	3.08	75.6	29.9
"	2.20	76.3	28.8
"	.655	77.4	31.6
"	.348	77.5	32.1
"	.176	77.3	31.1

LIST OF ILLUSTRATIONS

Figure 2

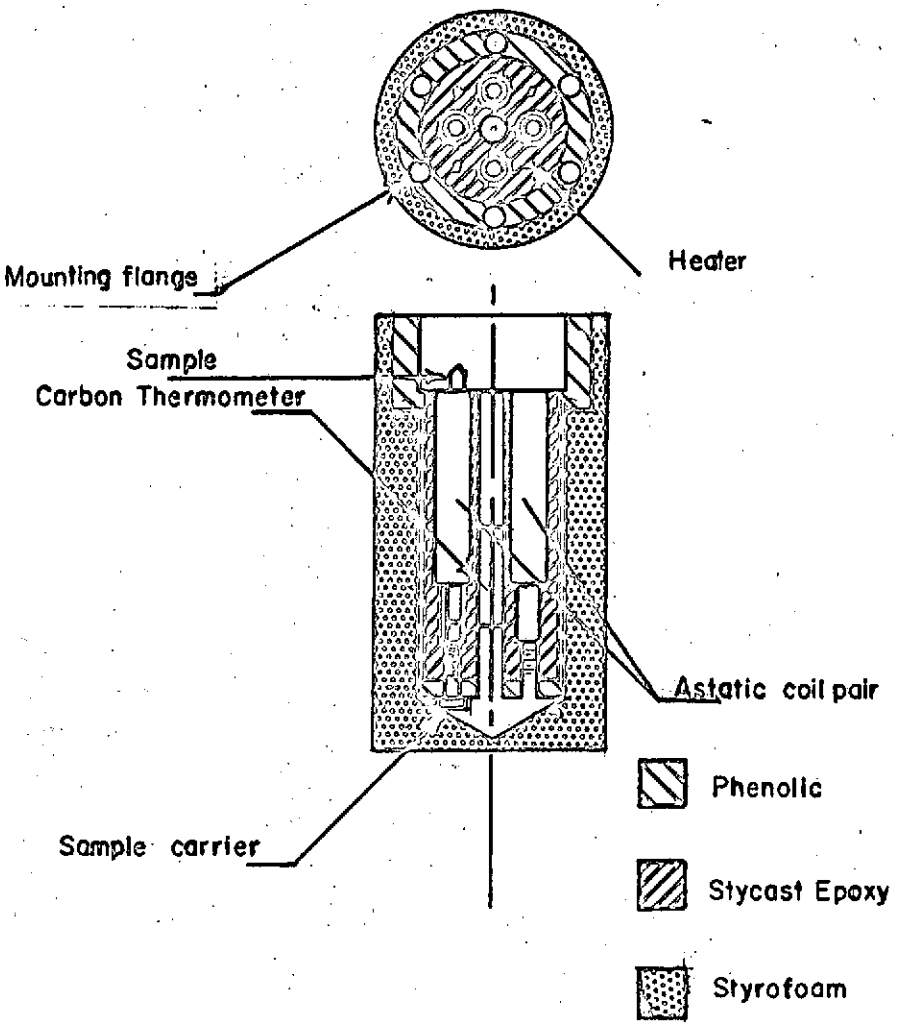

Magnetometer Tip

BLOCK DIAGRAM

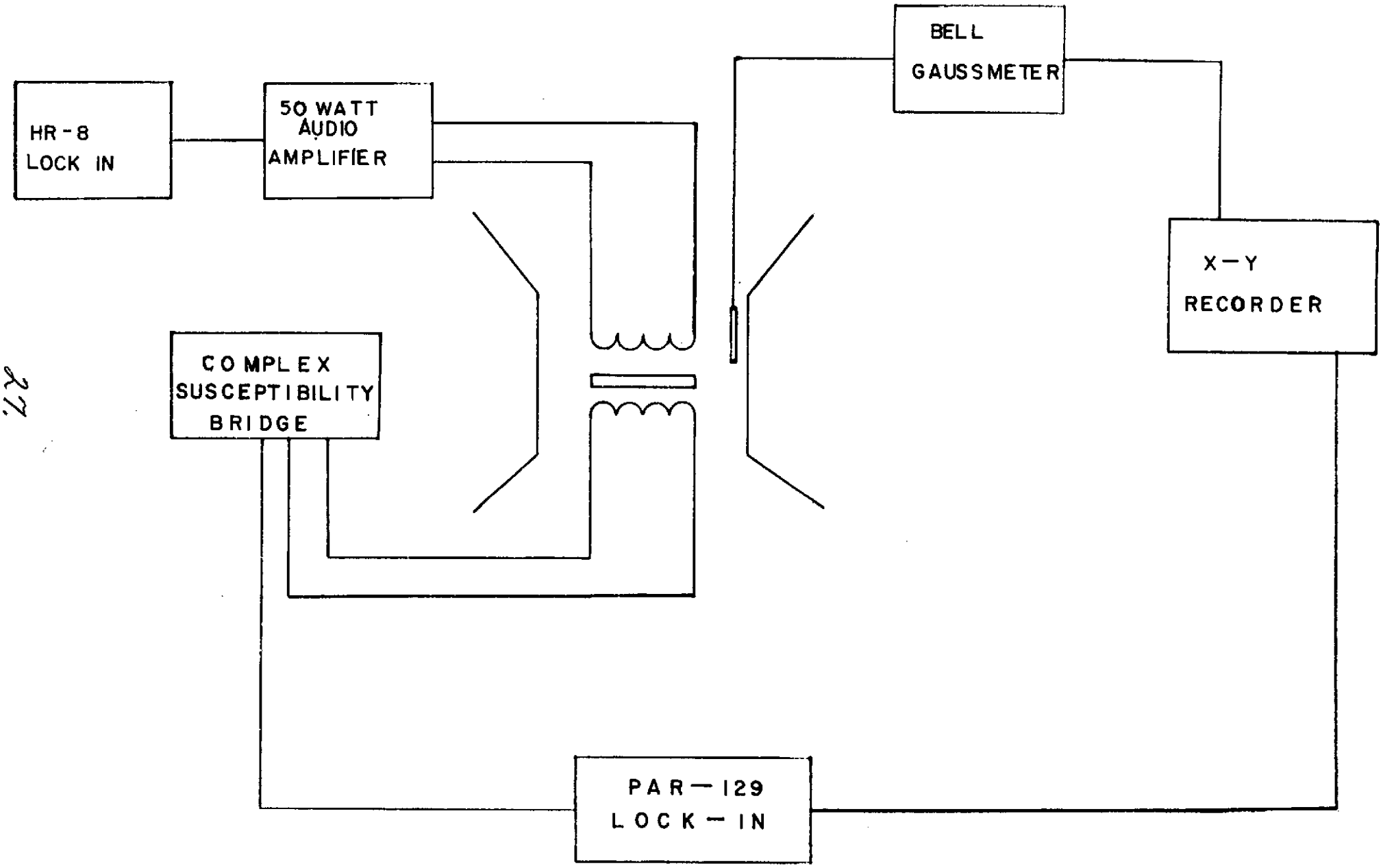

MODIFIED HARTSHORN BRIDGE

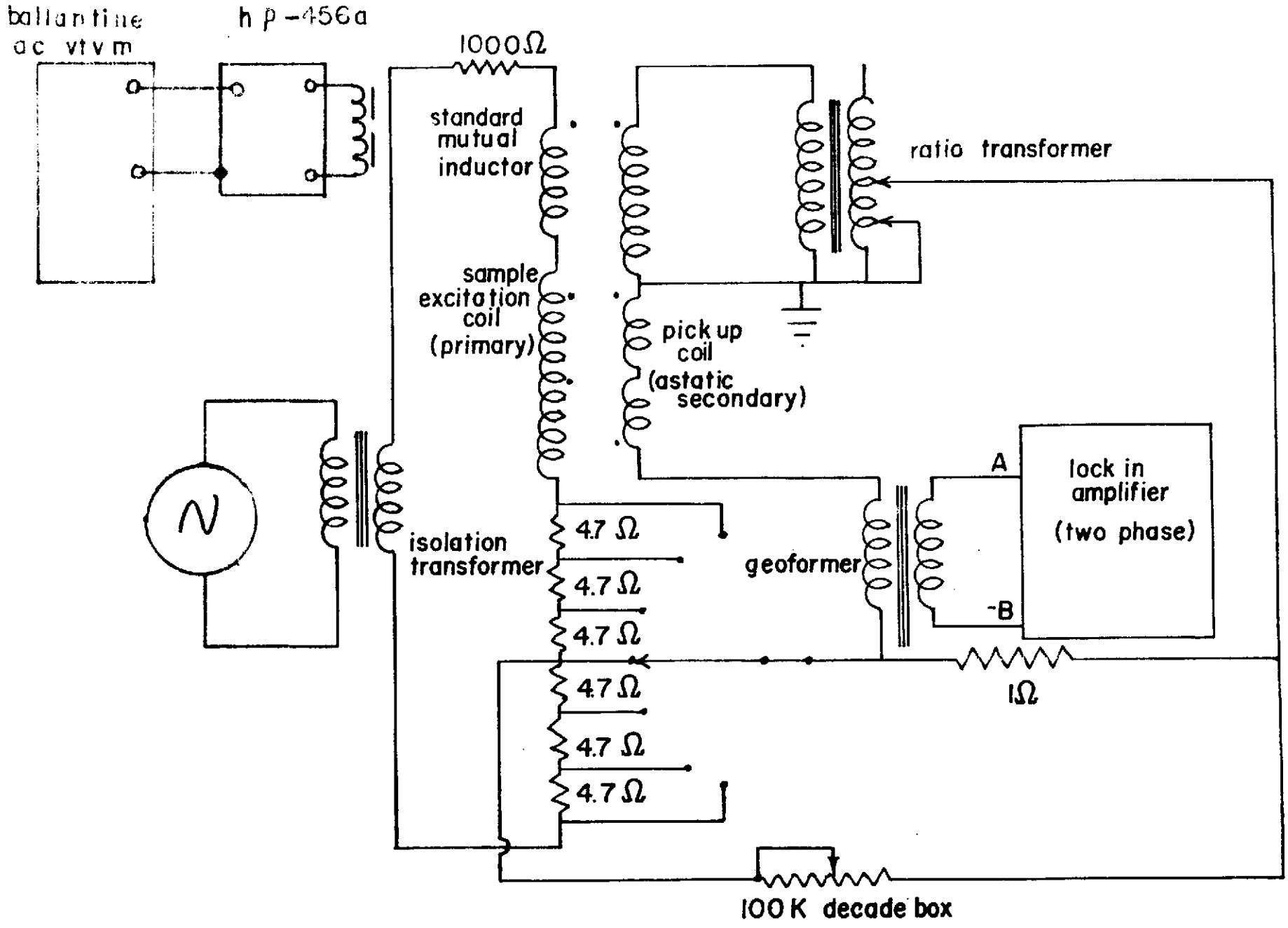

28

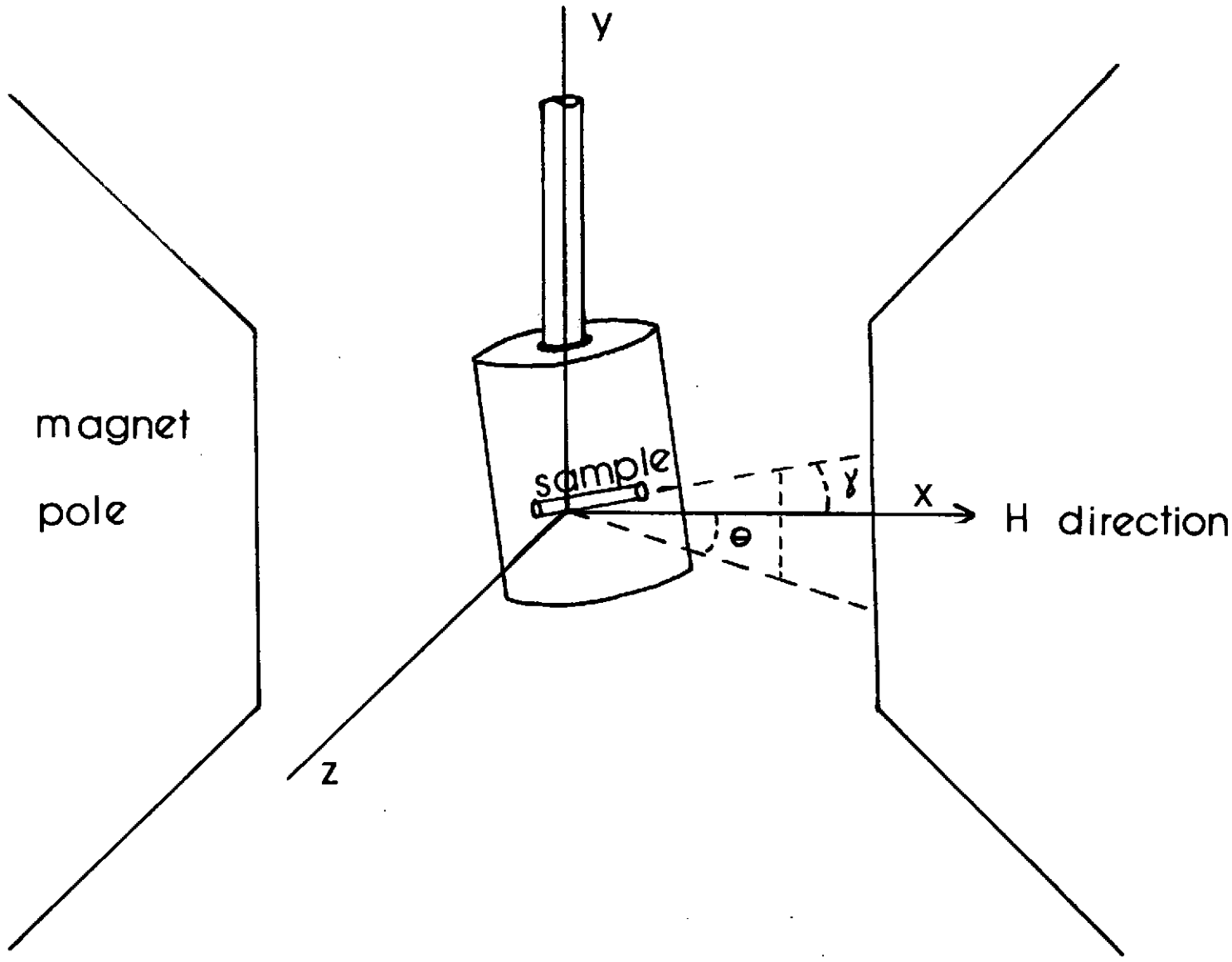

SAMPLE ALIGNMENT

$\chi'(\theta)$ - VS - H

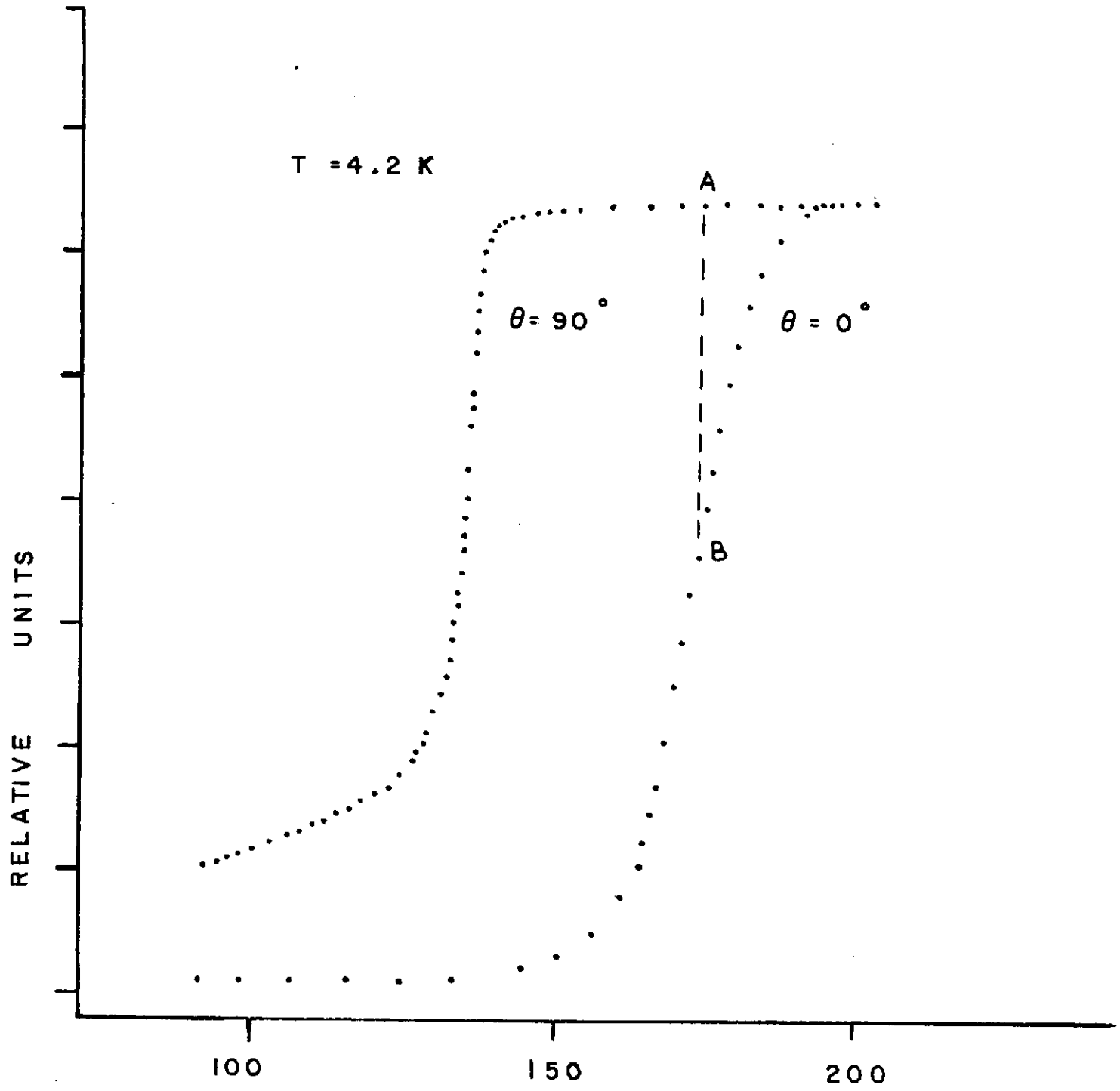

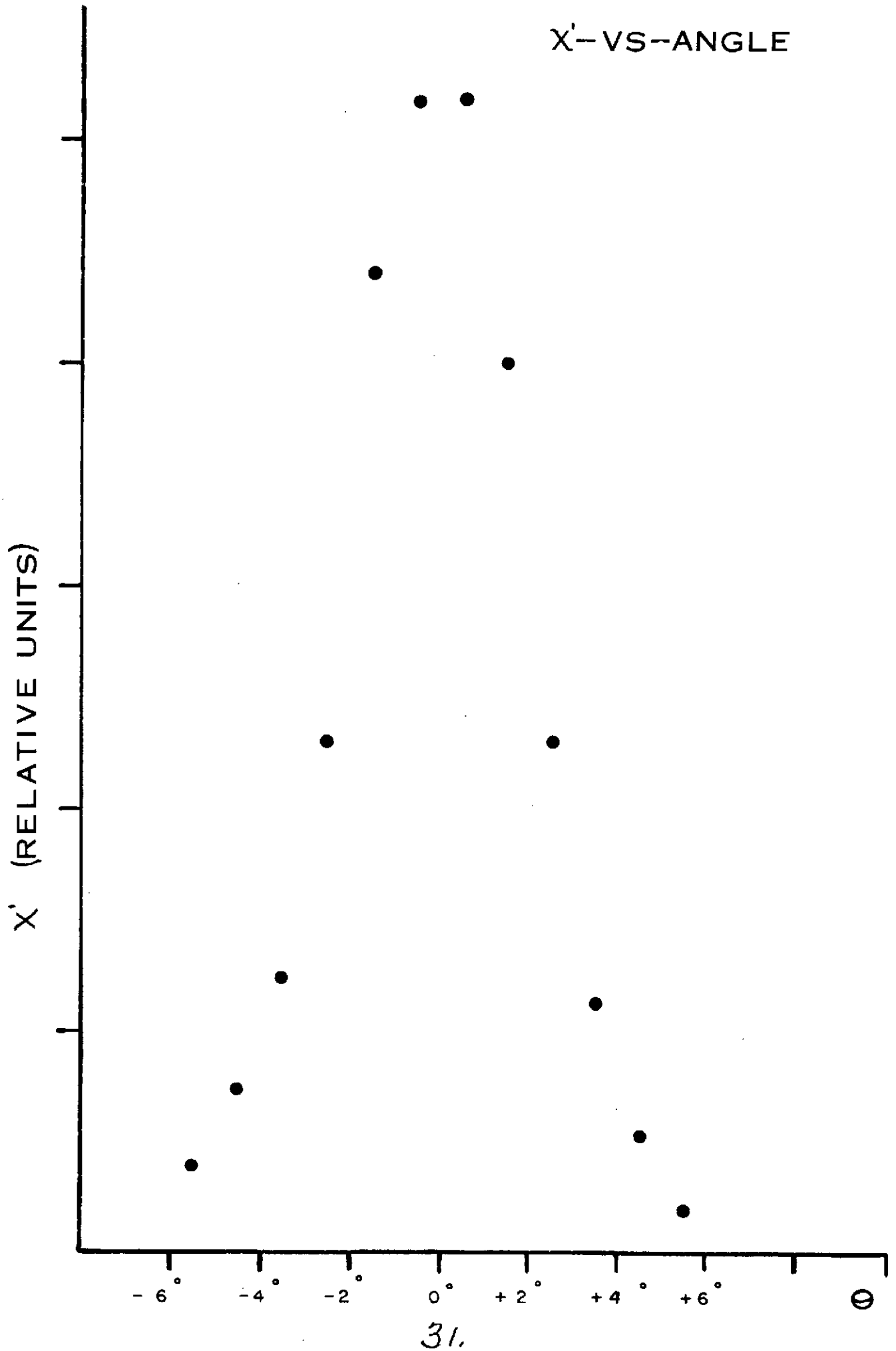
X'-VS-ANGLE
X' (RELATIVE UNITS)
- 6°
-4°
-2°
0°
+ 2°
+4°
+6°
θ

Figure 8

Resistivity Apparatus

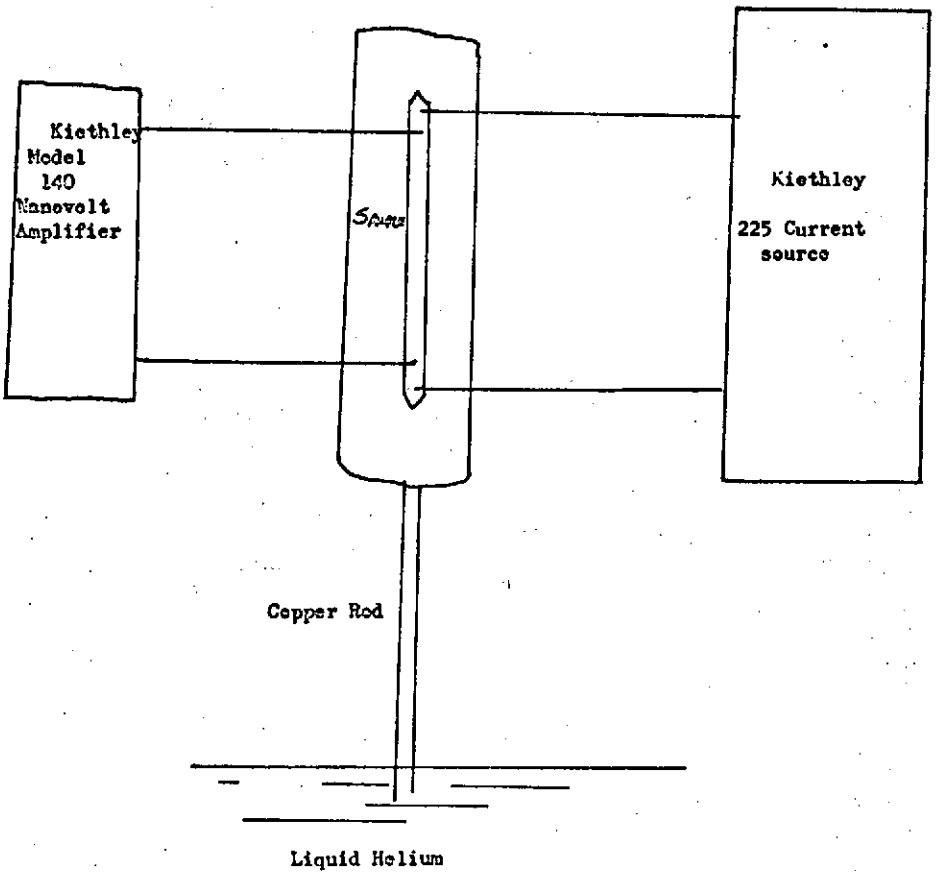

Figure 9

Electropolishing Arrangement

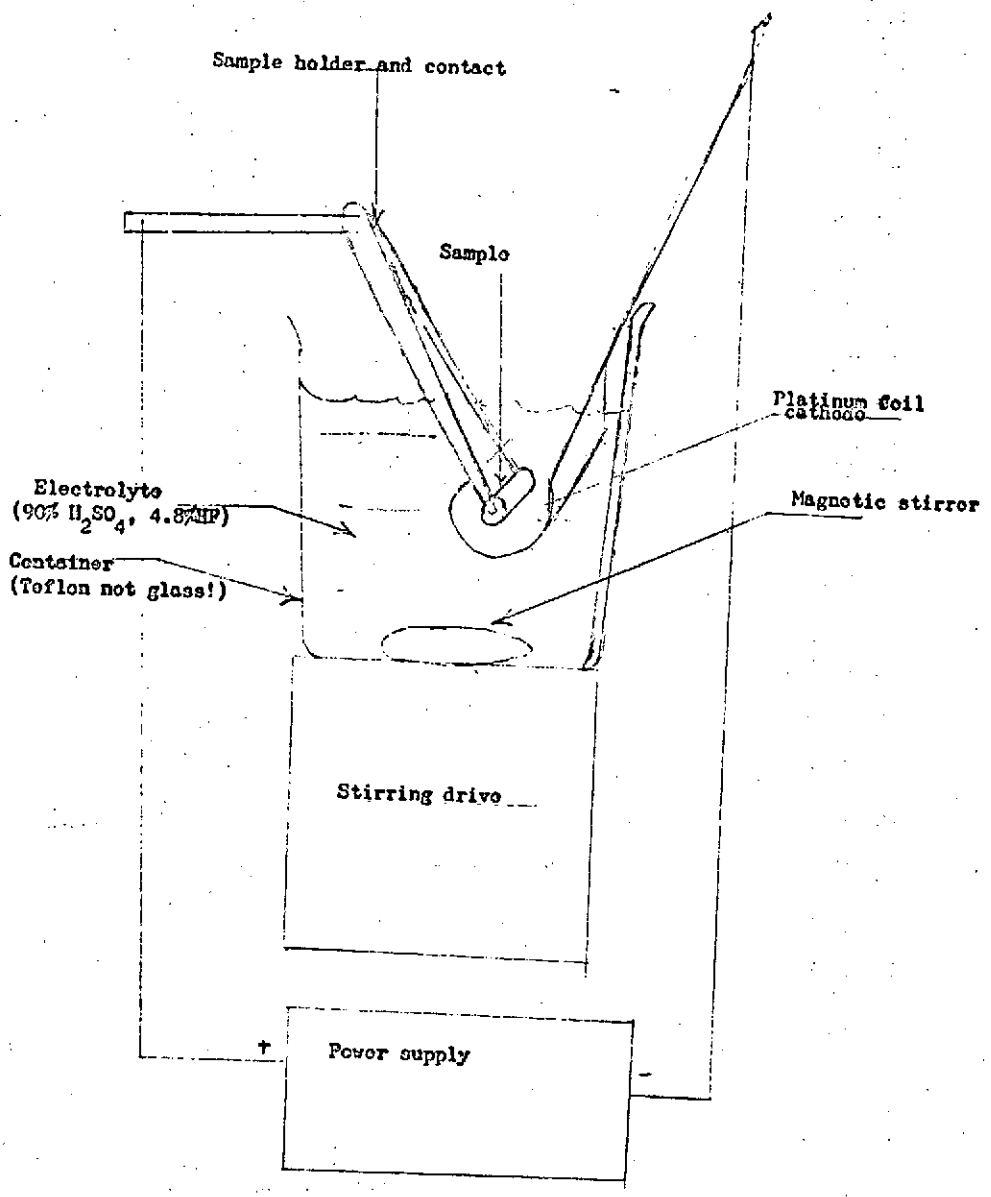

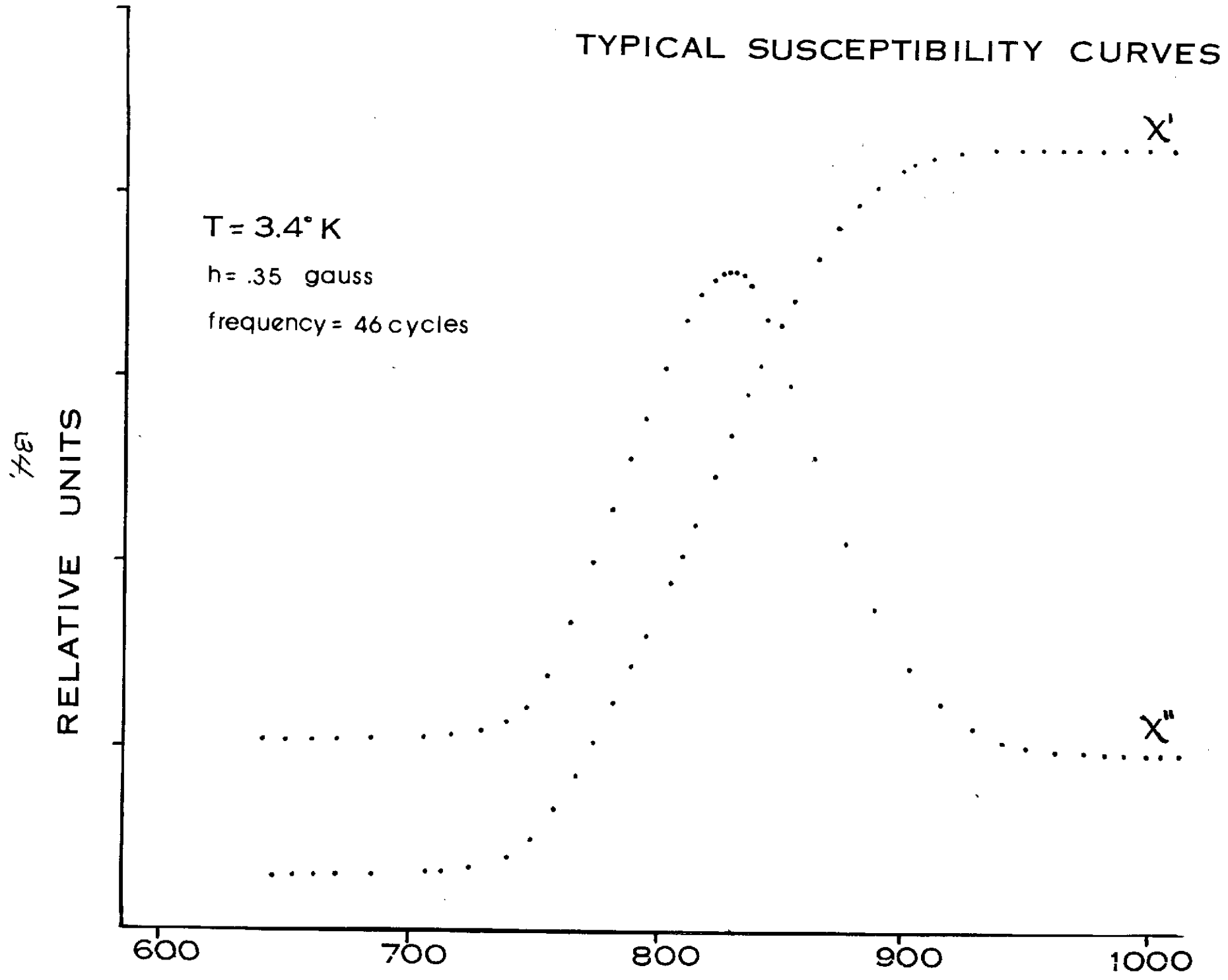
TYPICAL SUSCEPTIBILITY CURVES
T = 3.4° K
h = .35 gauss
frequency = 46 cycles
χ'
χ"
RELATIVE UNITS
600
700
800
900
1000

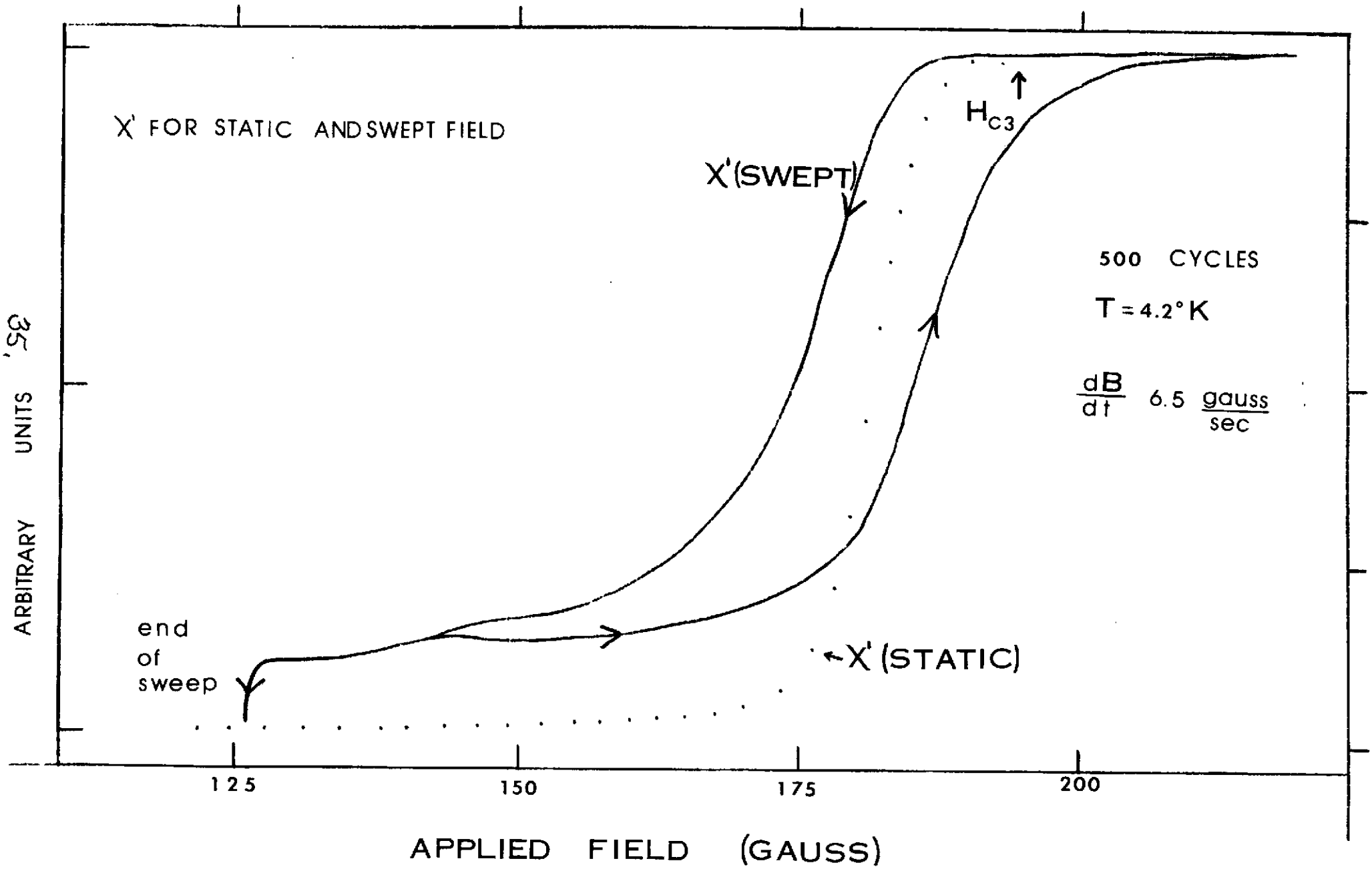
X' FOR STATIC AND SWEPT FIELD
X'(SWEPT)
H_{c3}
500 CYCLES
T = 4.2° K
$\frac{dB}{dt}$ 6.5 $\frac{gauss}{sec}$
end of sweep
X' (STATIC)
ARBITRARY UNITS
125
150
175
200
APPLIED FIELD (GAUSS)

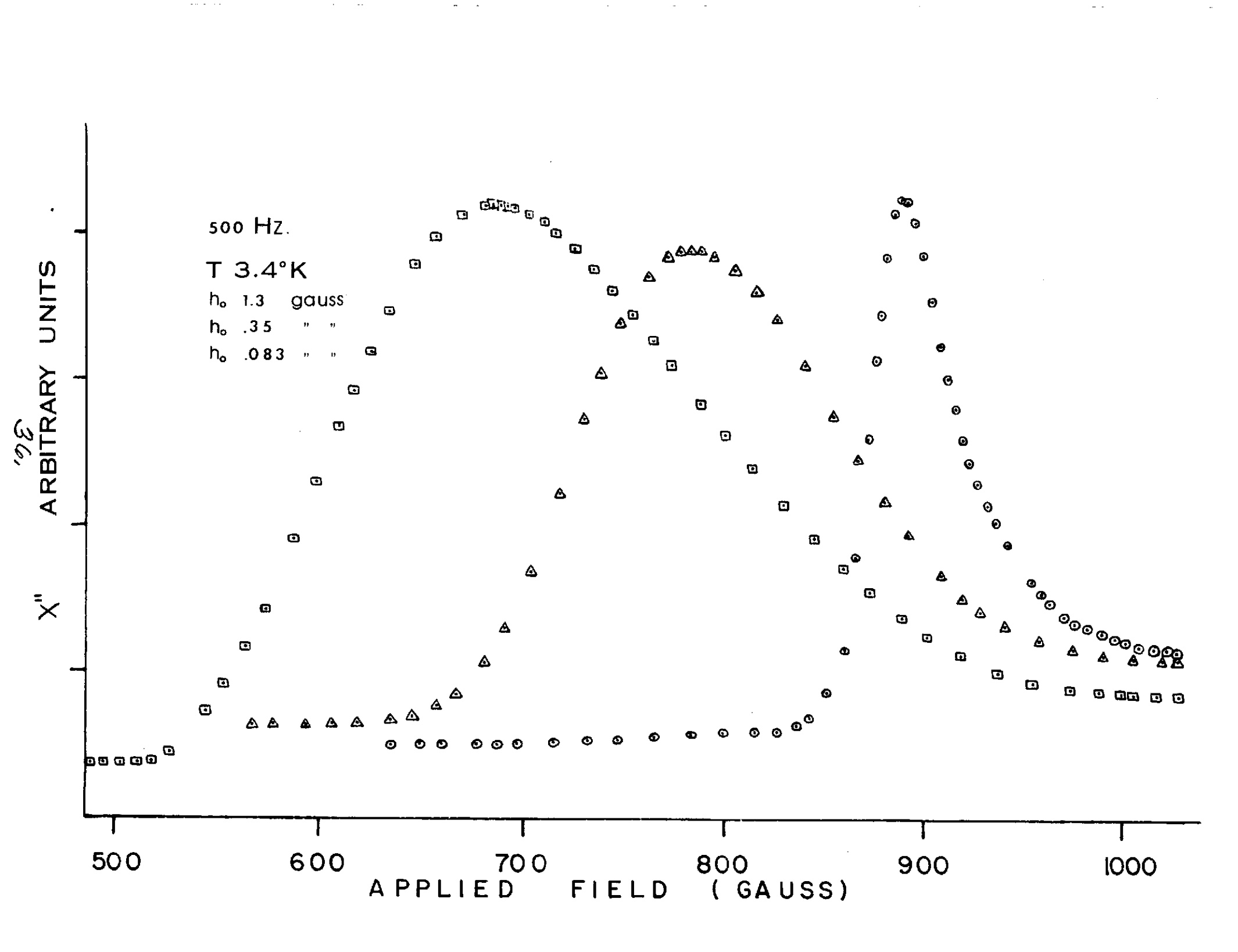
500 Hz.
T 3.4°K
h_o 1.3 gauss
h_o .35 " "
h_o .083 " "
X'' ARBITRARY UNITS
500
600
700
800
900
1000
APPLIED FIELD (GAUSS)

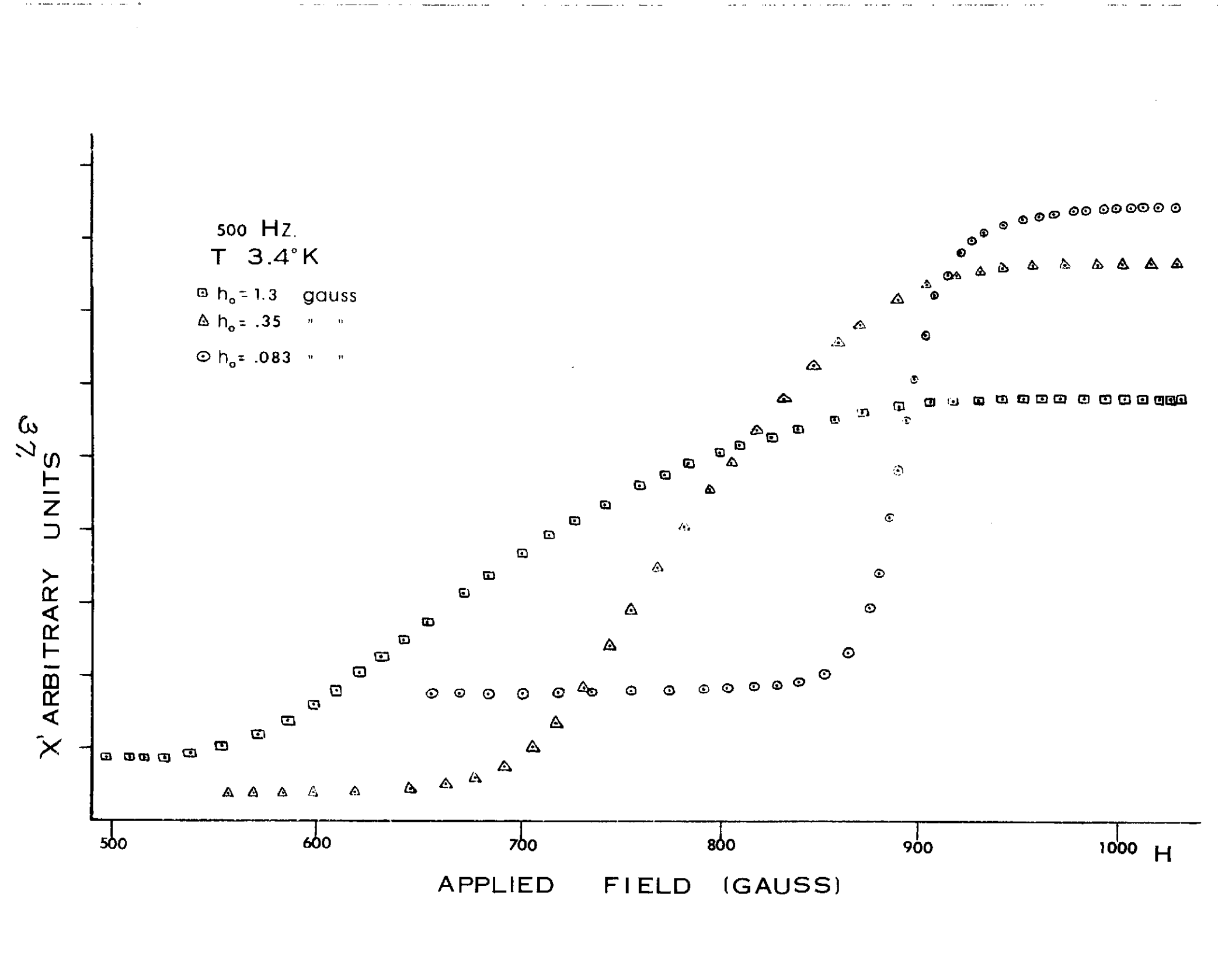
500 Hz.
T 3.4°K
h_o = 1.3 gauss
h_o = .35 " "
h_o = .083 " "
χ' ARBITRARY UNITS
500
600
700
800
900
1000
H
APPLIED FIELD (GAUSS)

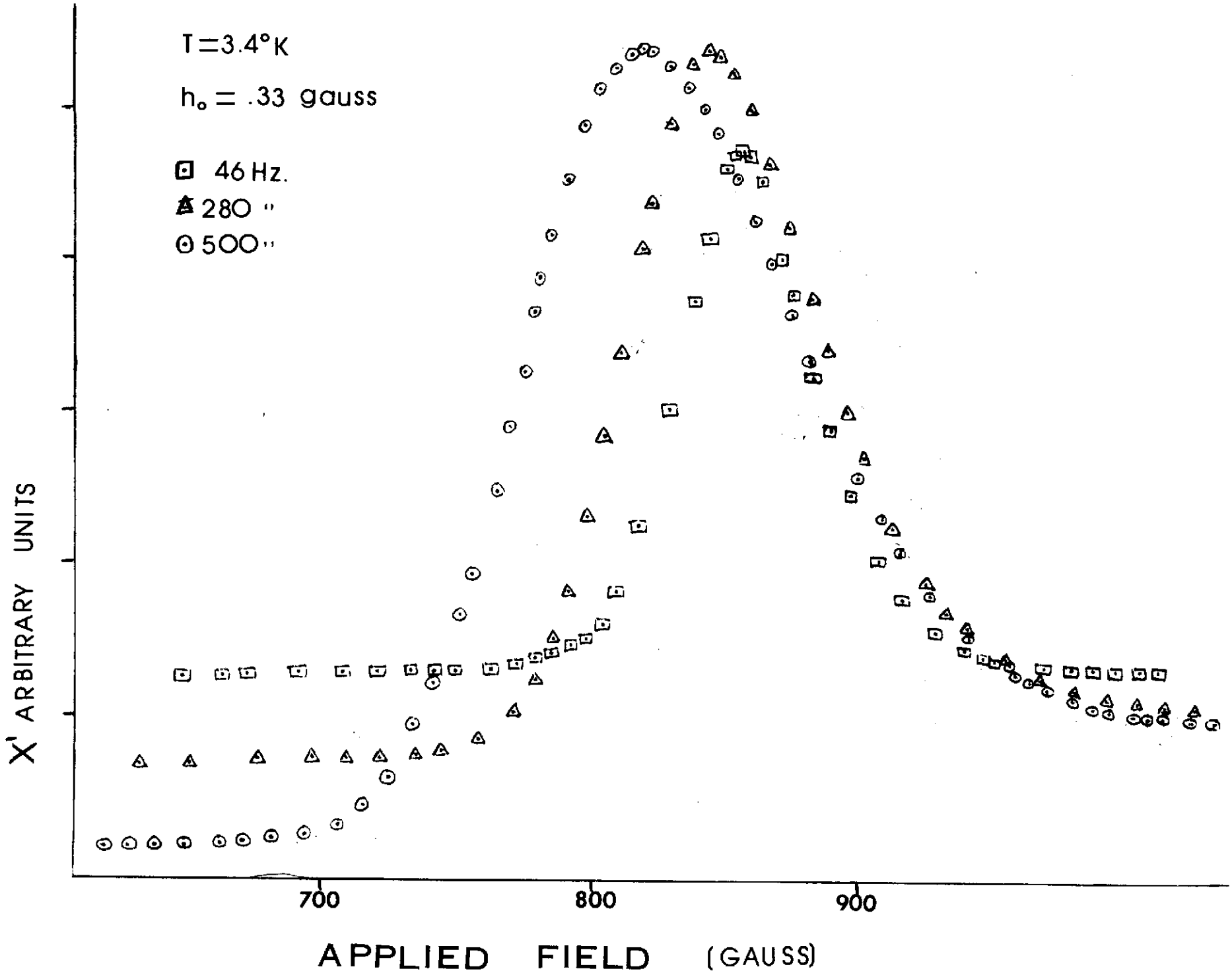
T=3.4°K
h_o = .33 gauss
46 Hz.
280 "
500 "
X' ARBITRARY UNITS
700
800
900
APPLIED FIELD (GAUSS)

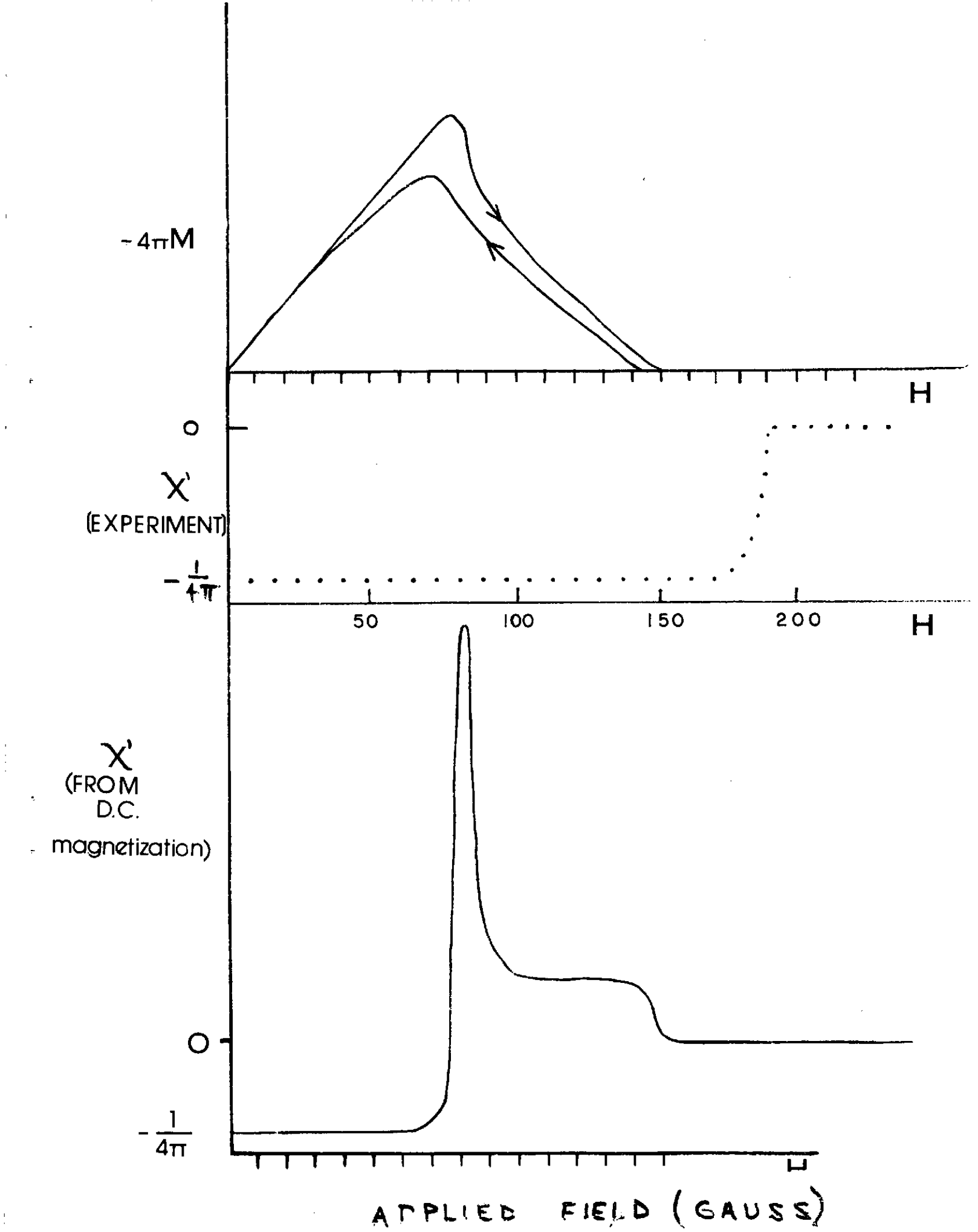
-4πM
H
0
χ'
(EXPERIMENT)
-1/4π
50
100
150
200
H
χ'
(FROM
D.C.
magnetization)
0
-1/4π
H
APPLIED FIELD (GAUSS)

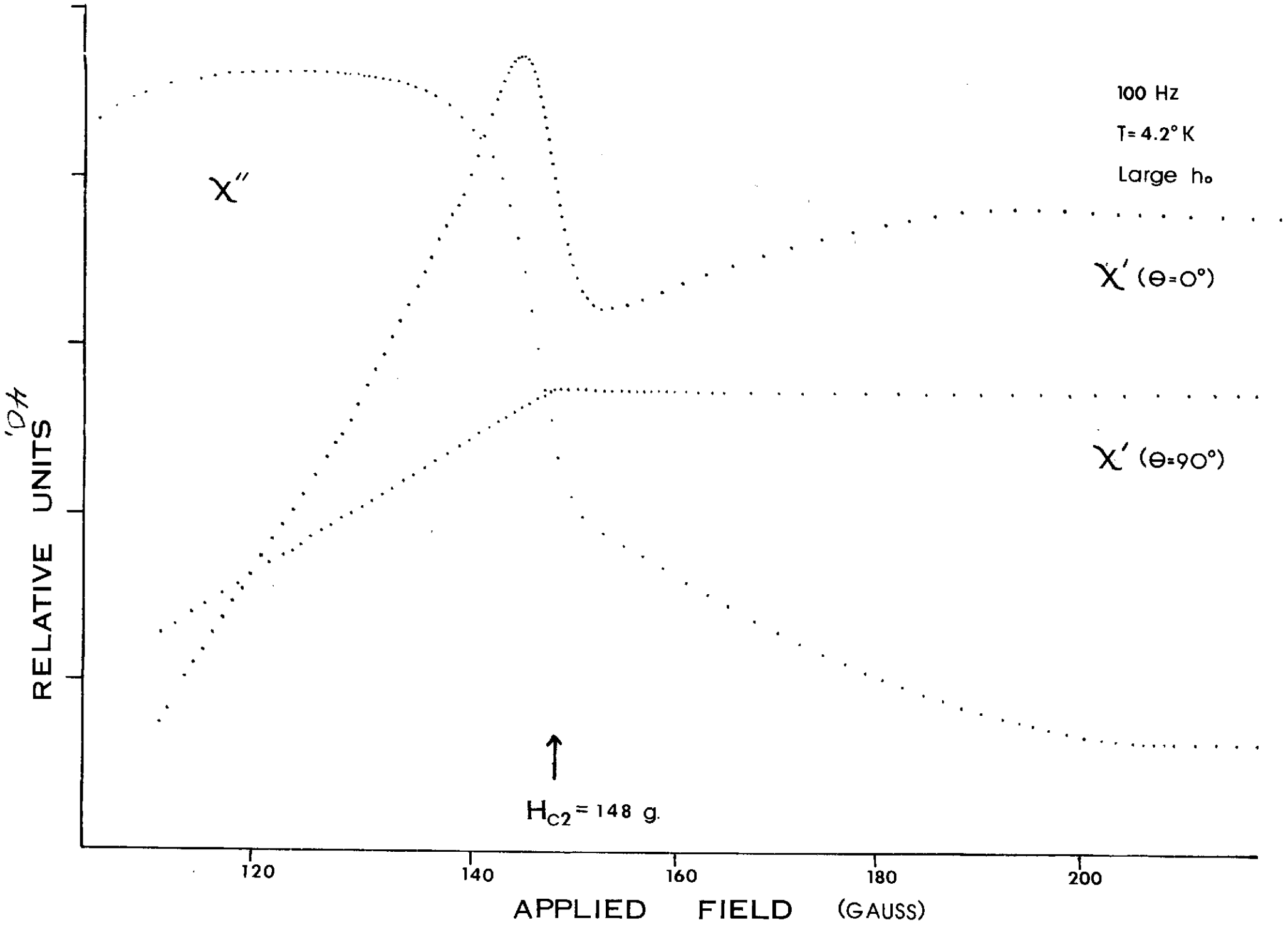
100 Hz
T= 4.2° K
Large h_o
χ″
χ′ (θ=0°)
χ′ (θ=90°)
RELATIVE UNITS
H_{C2} = 148 g.
120
140
160
180
200
APPLIED FIELD (GAUSS)

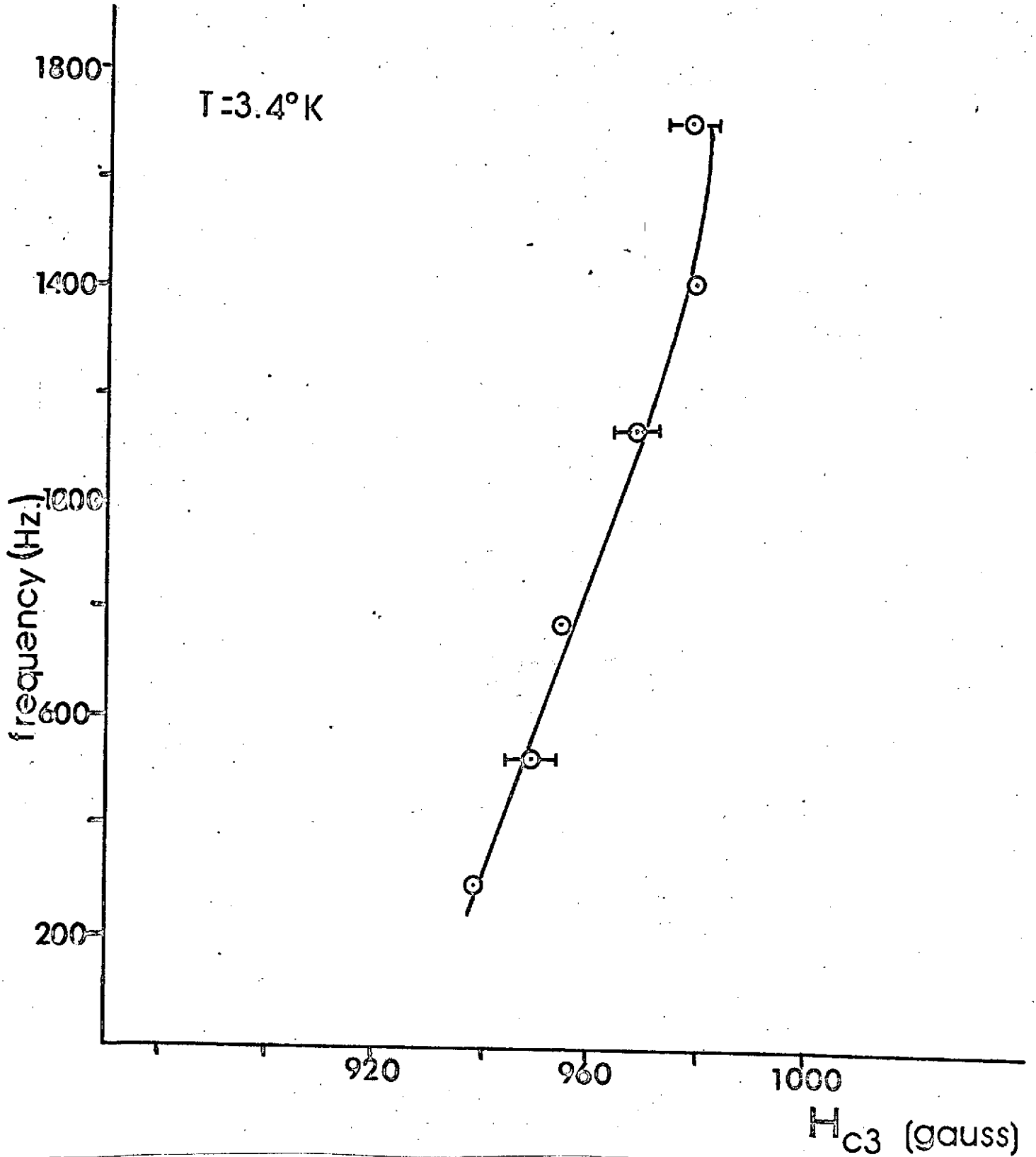
T=3.4°K
1800
1400
1000
600
200
frequency (Hz.)
920
960
1000
H_{c3} (gauss)

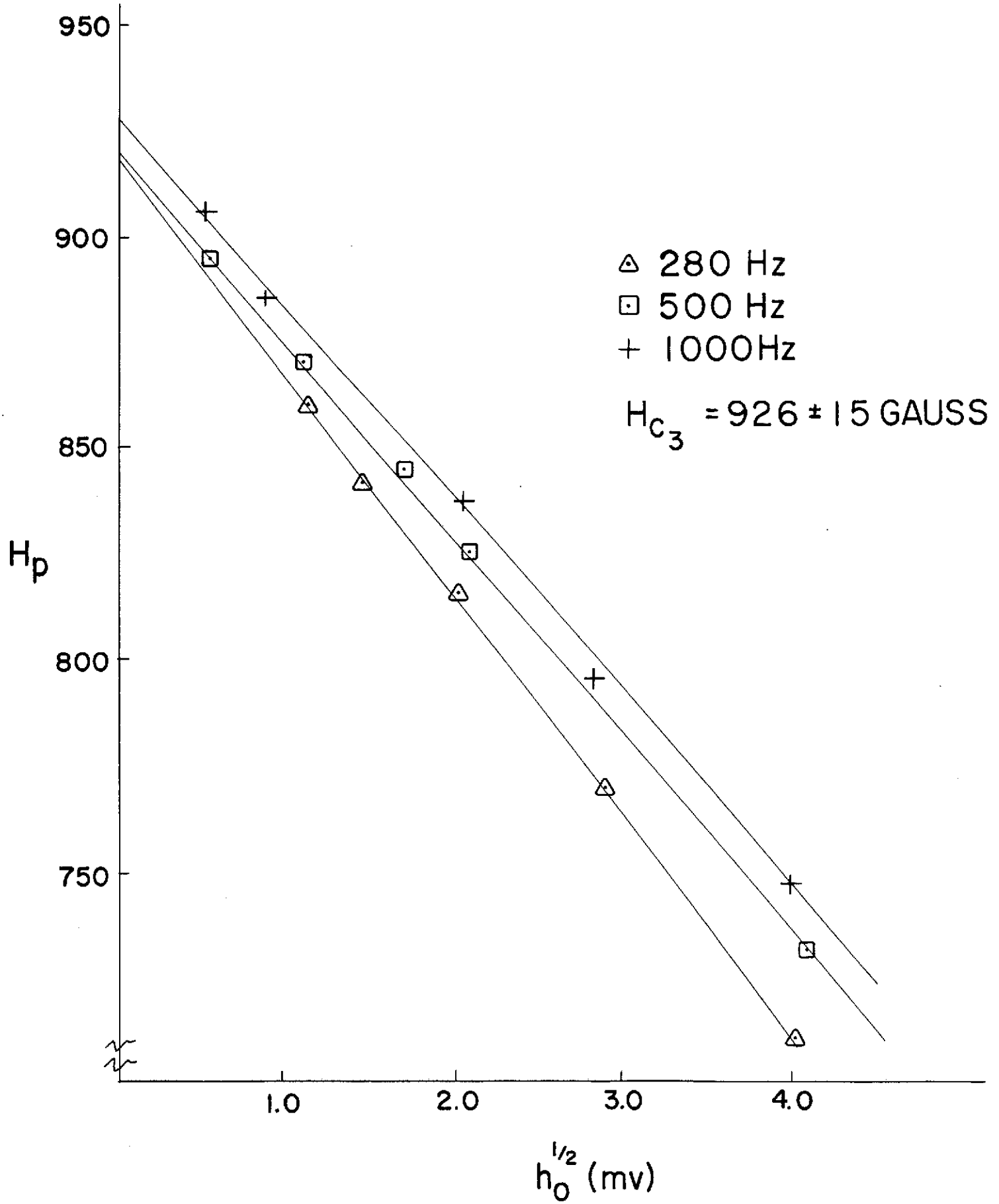
950
900
850
800
750
H_p
△ 280 Hz
⊡ 500 Hz
+ 1000Hz
H_{c_3} = 926 ± 15 GAUSS
1.0
2.0
3.0
4.0
$h_0^{1/2}$ (mv)

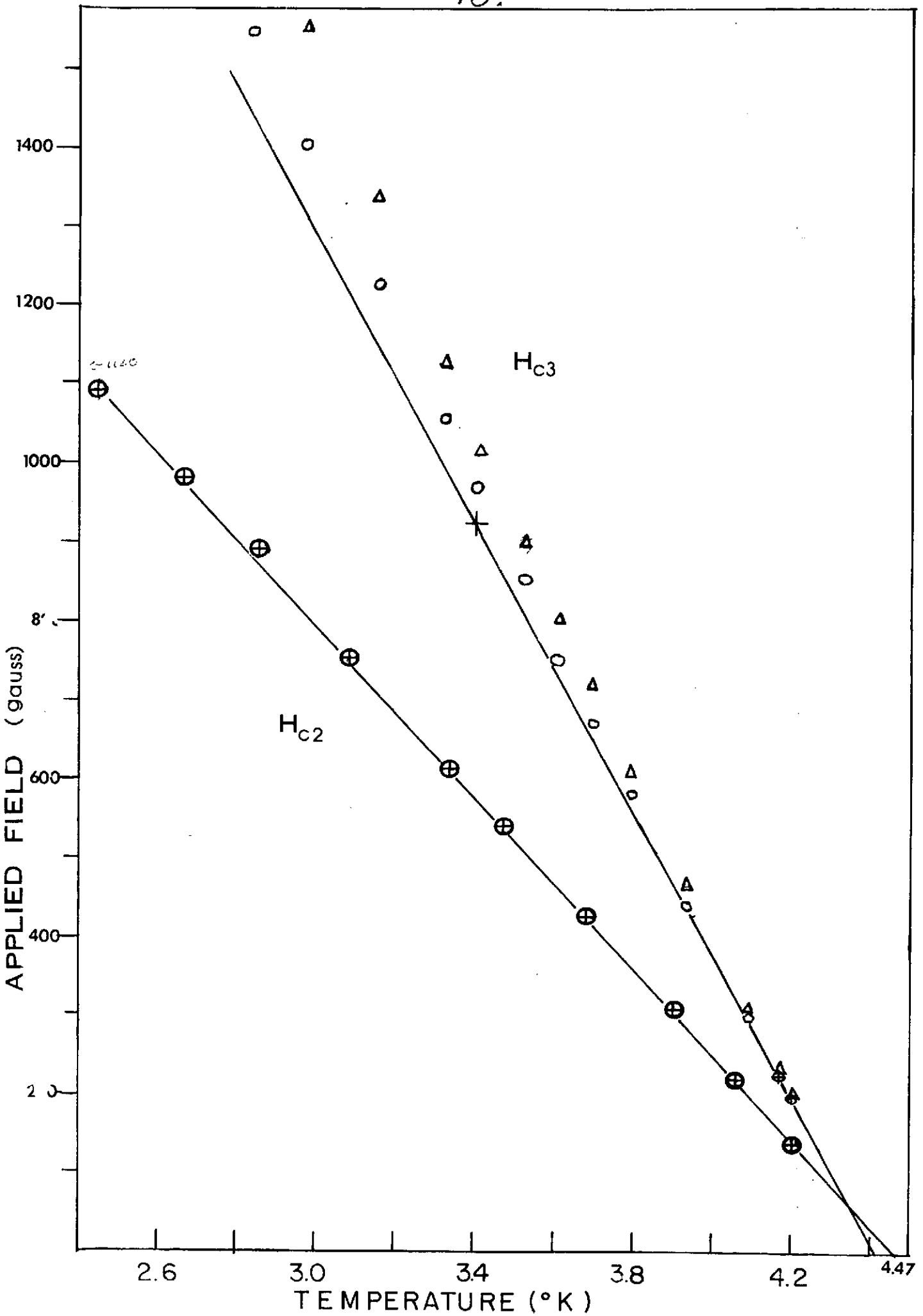
1400
1200
1000
800
600
400
200
APPLIED FIELD (gauss)
H_{c3}
H_{c2}
2.6
3.0
3.4
3.8
4.2
4.47
TEMPERATURE (°K)

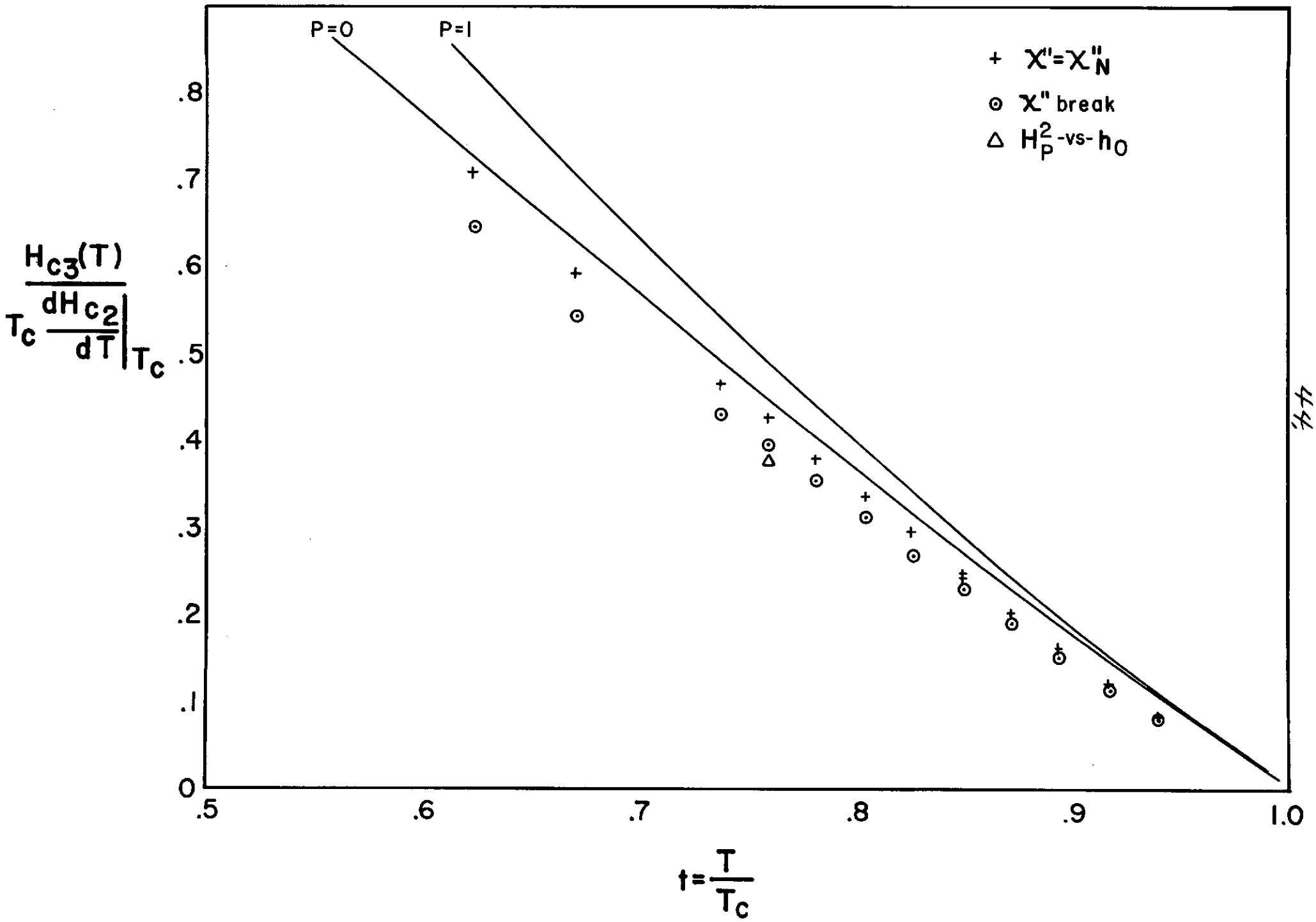
P=0
P=1
+ χ'=χ''N
⊙ χ'' break
△ H²P-vs-h0
.8
.7
.6
.5
.4
.3
.2
.1
0
.5
.6
.7
.8
.9
1.0
Hc3(T) / Tc dHc2/dT |Tc
t=T/Tc

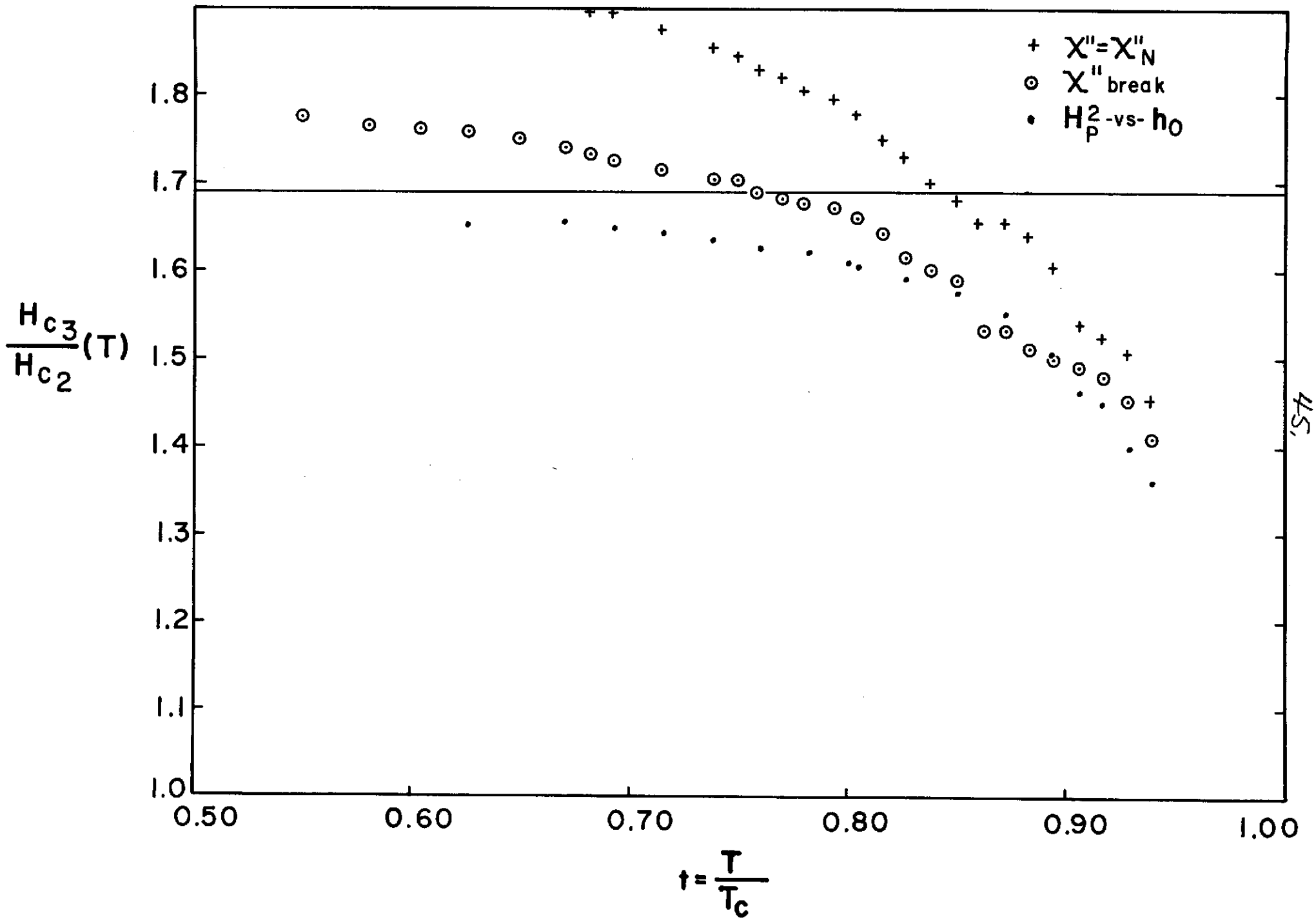
χ''=χ''N
χ''break
H²p-vs-h0
Hc3/Hc2(T)
1.8
1.7
1.6
1.5
1.4
1.3
1.2
1.1
1.0
0.50
0.60
0.70
0.80
0.90
1.00
t = T/Tc
45'

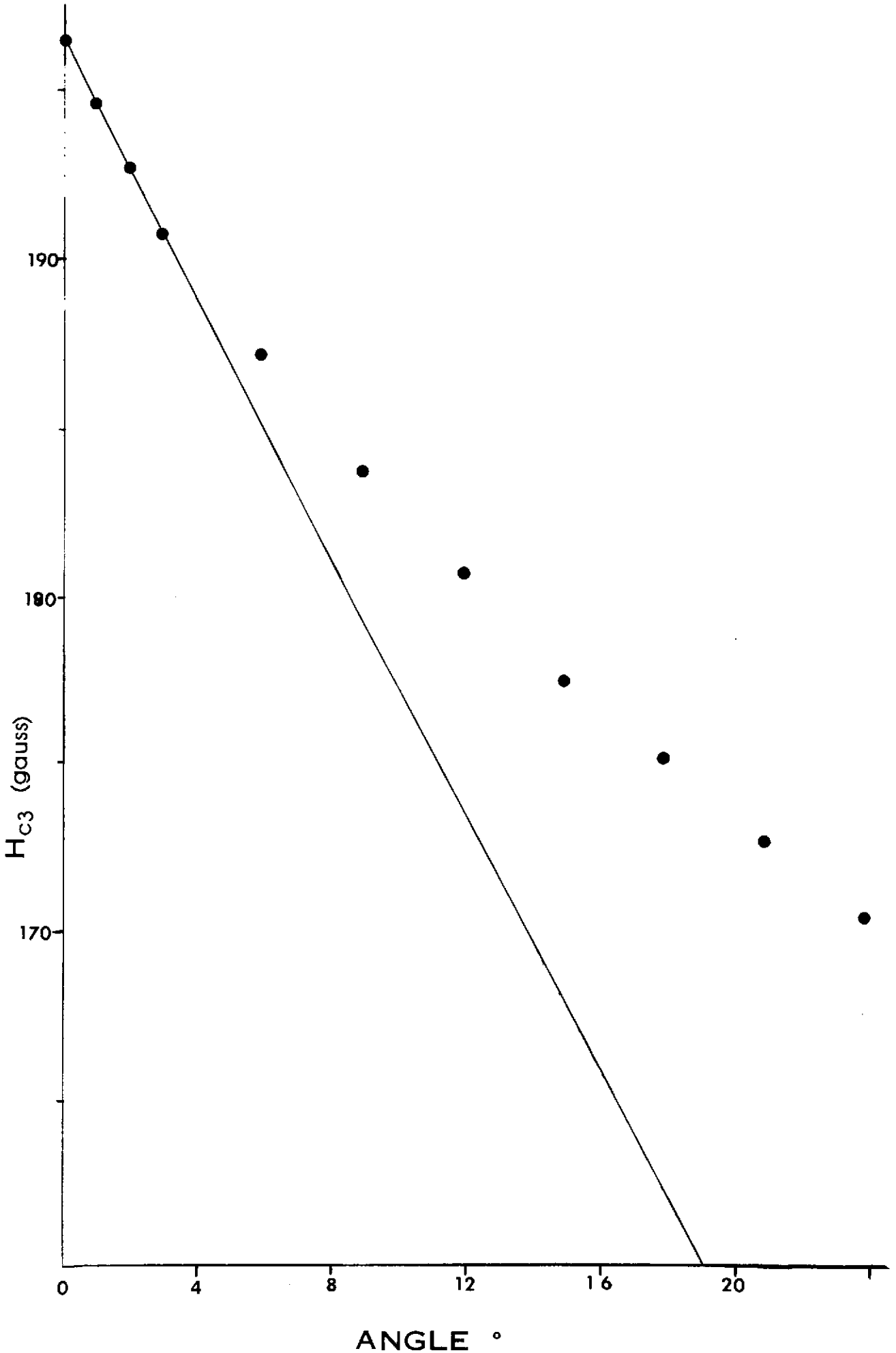
190
180
170
H_{c3} (gauss)
0
4
8
12
16
20
ANGLE °

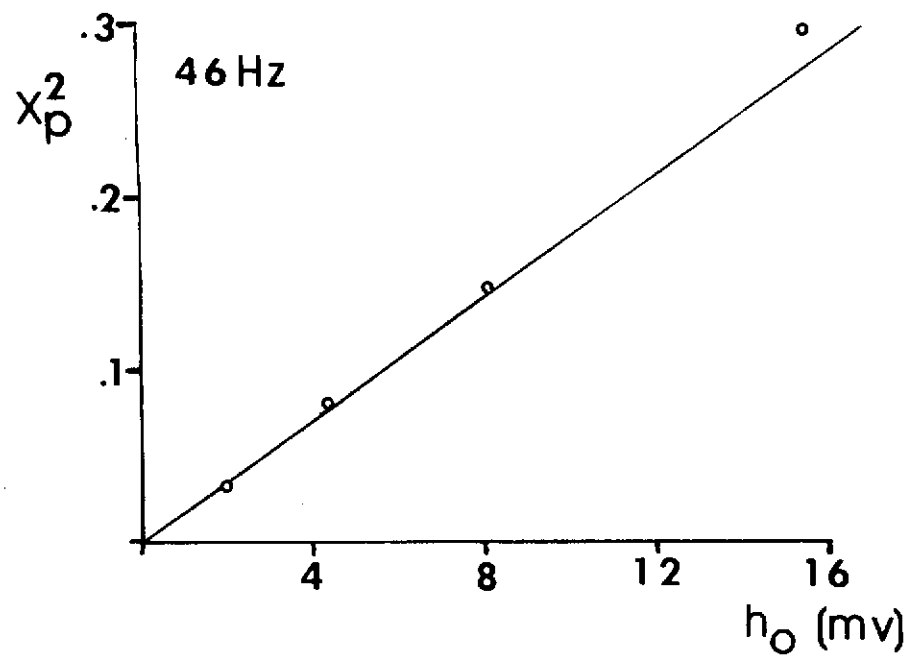

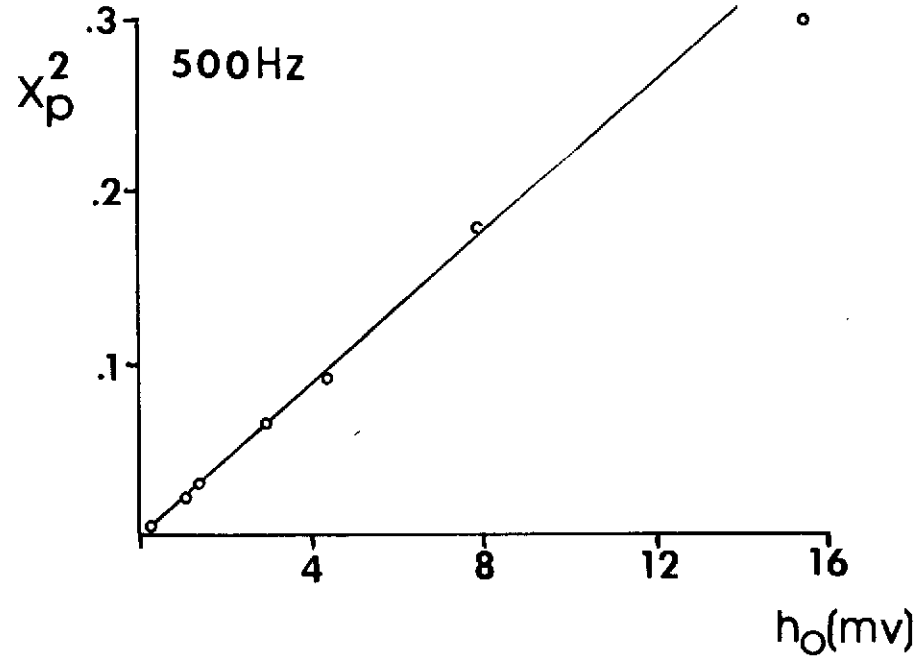

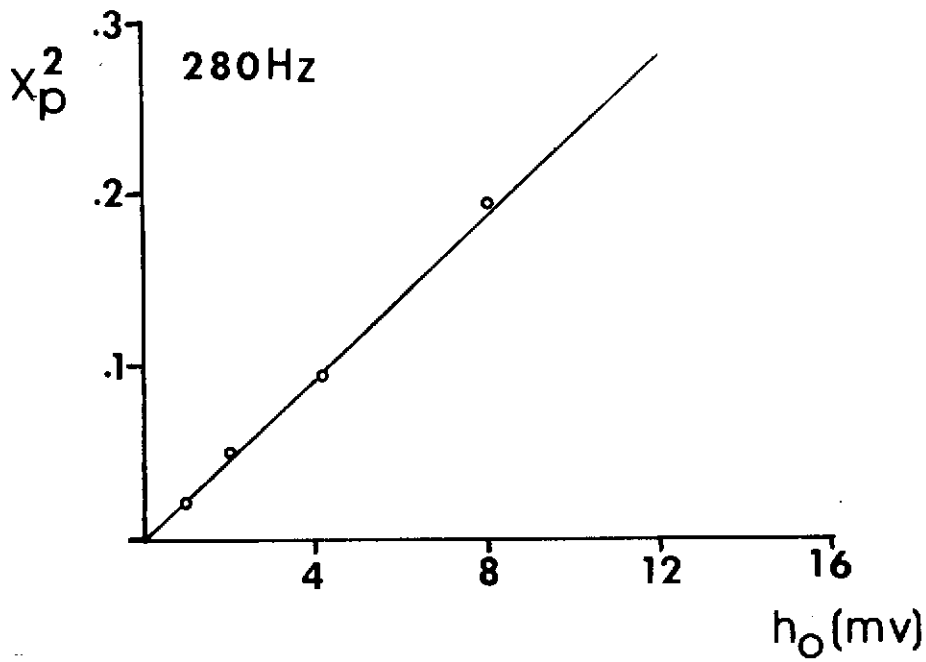

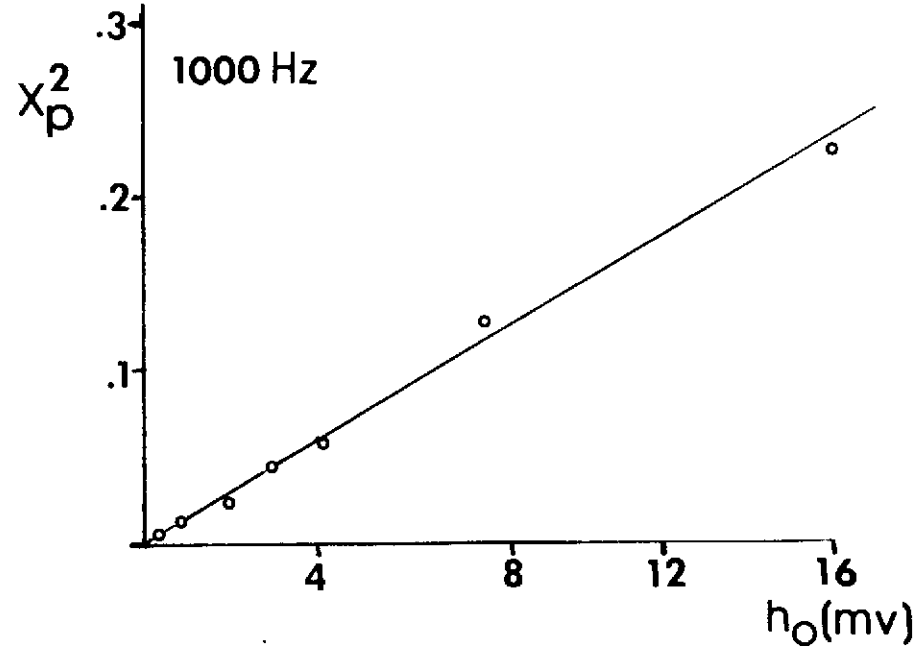

T= 3.4°K

12 mv=1.99 gauss

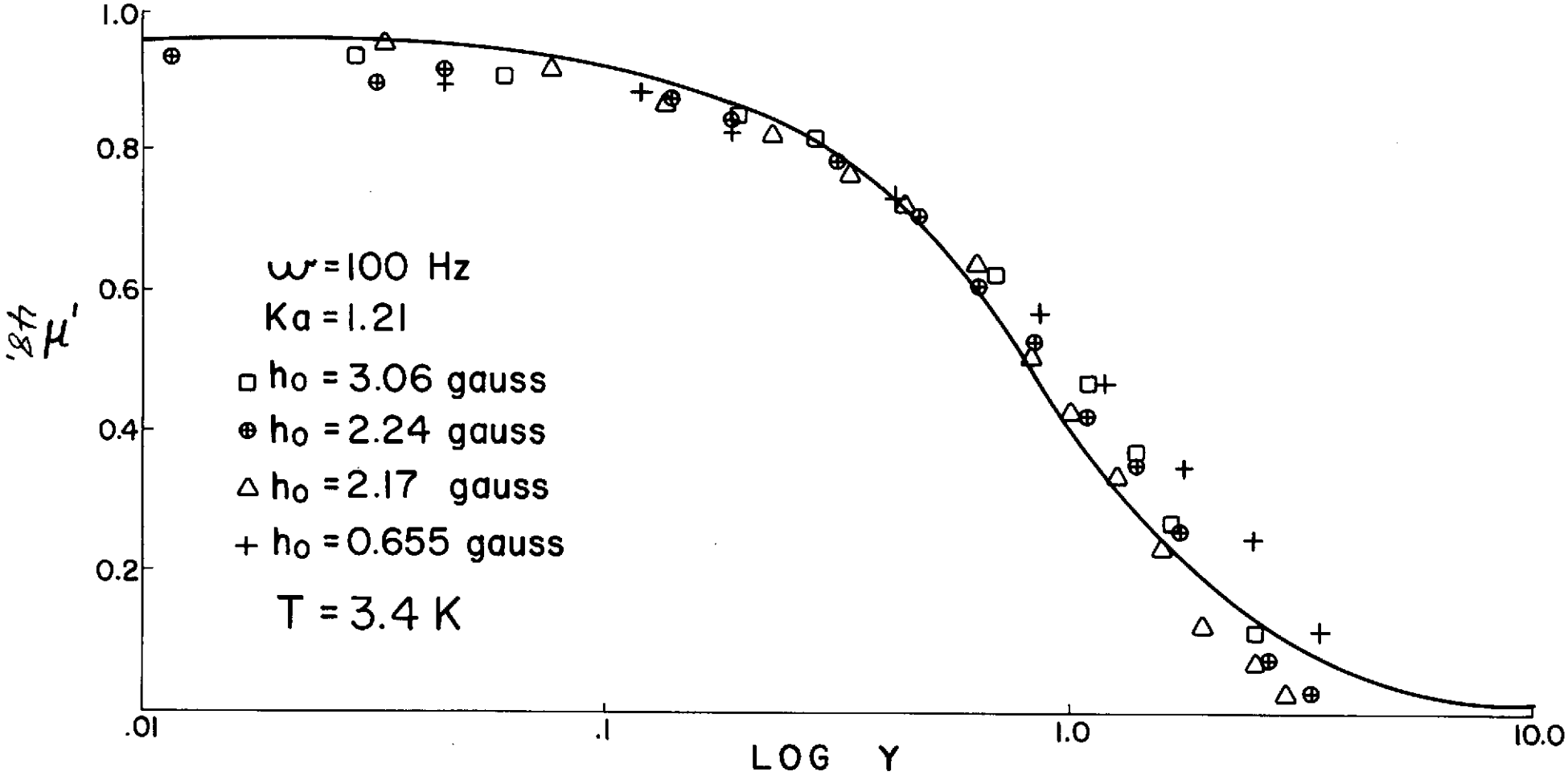
1.0
0.8
0.6
0.4
0.2
'84 μ'
ω = 100 Hz
Ka = 1.21
□ h₀ = 3.06 gauss
⊕ h₀ = 2.24 gauss
△ h₀ = 2.17 gauss
+ h₀ = 0.655 gauss
T = 3.4 K
.01
.1
1.0
10.0
LOG Y

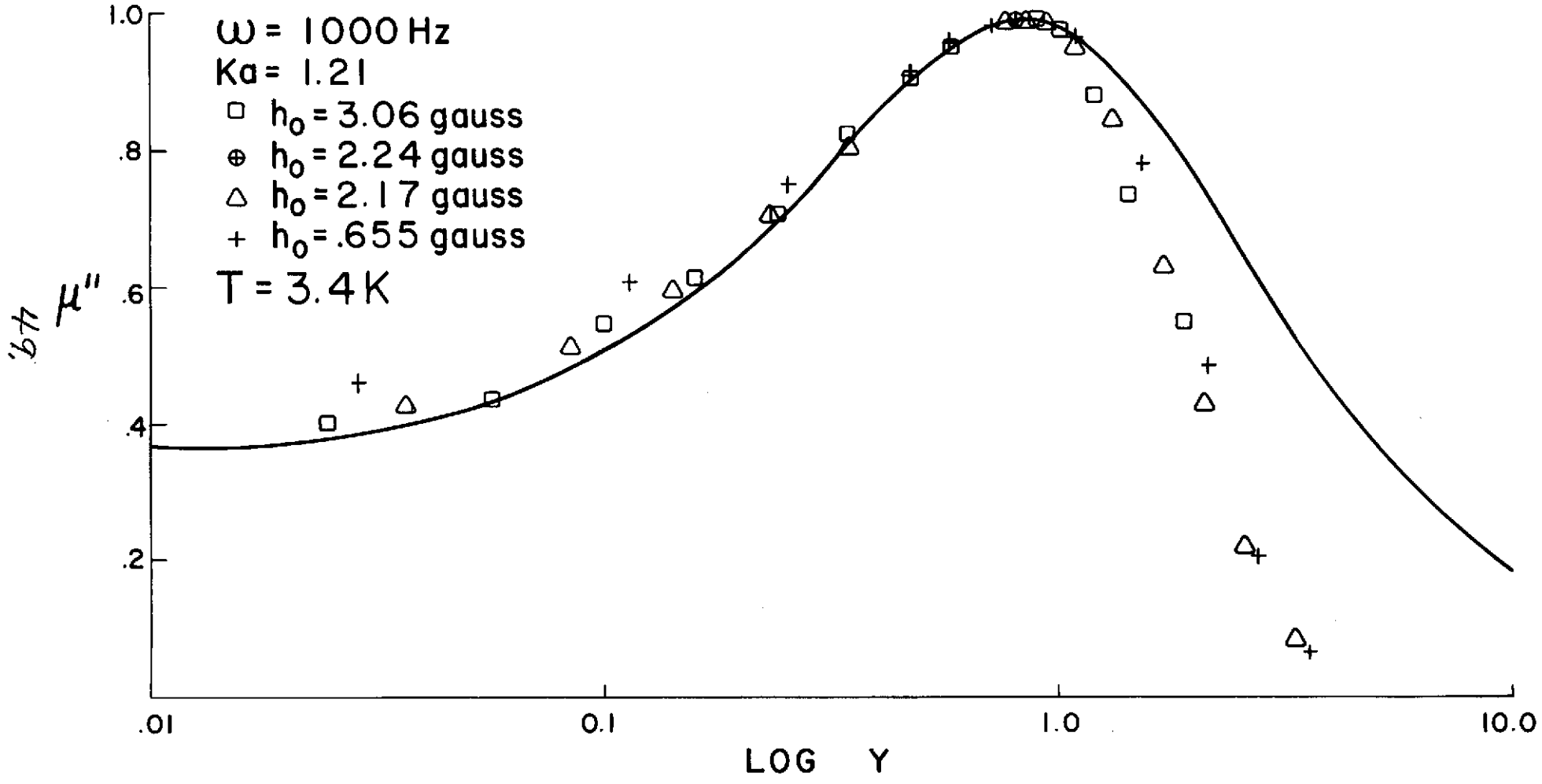
ω = 1000 Hz
Ka = 1.21
□ h0 = 3.06 gauss
⊕ h0 = 2.24 gauss
△ h0 = 2.17 gauss
+ h0 = .655 gauss
T = 3.4 K
'bh μ''
1.0
.8
.6
.4
.2
.01
0.1
1.0
10.0
LOG Y

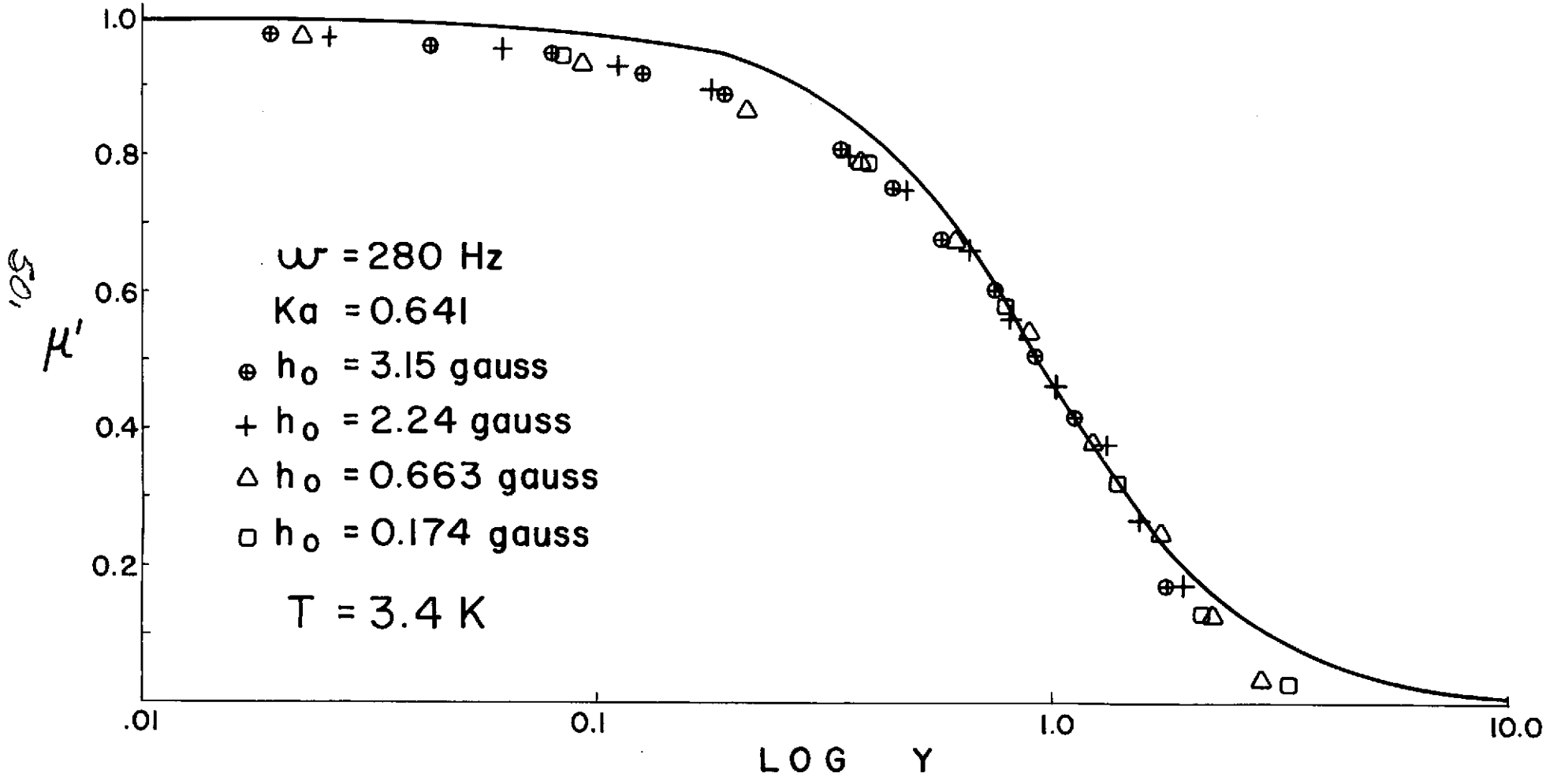
1.0
0.8
0.6
0.4
0.2
μ'
ω = 280 Hz
Ka = 0.641
⊕ h₀ = 3.15 gauss
+ h₀ = 2.24 gauss
△ h₀ = 0.663 gauss
□ h₀ = 0.174 gauss
T = 3.4 K
.01
0.1
1.0
10.0
LOG Y

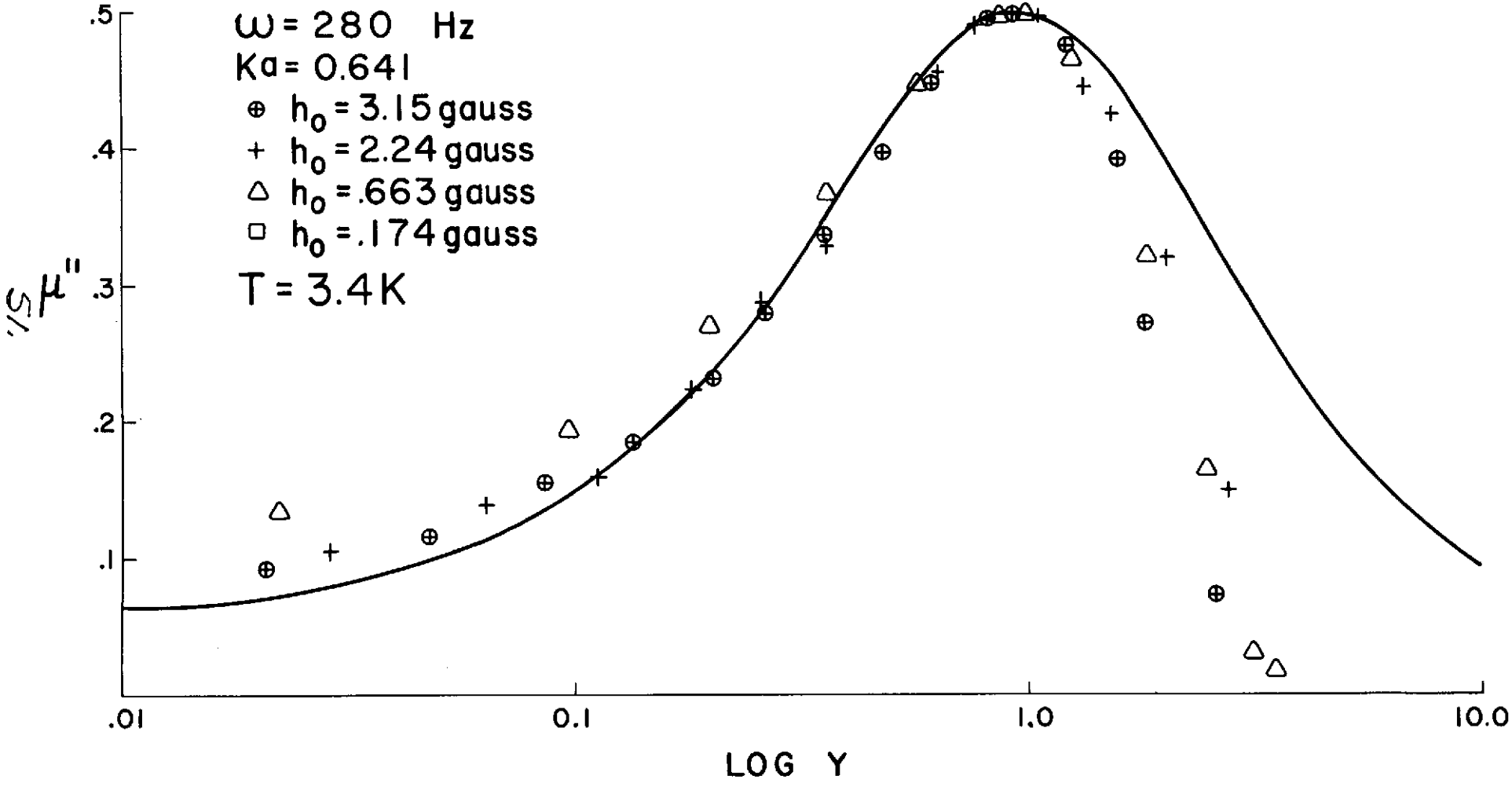
ω = 280 Hz
Ka = 0.641
⊕ h_0 = 3.15 gauss
+ h_0 = 2.24 gauss
△ h_0 = .663 gauss
□ h_0 = .174 gauss
T = 3.4K
.5
.4
.3
.2
.1
μ''
.01
0.1
1.0
10.0
LOG Y